NBS MONOGRAPH 143

U.S. DEPARTMENT OF COMMERCE / National Bureau of Standards

Analysis of Optically Excited Mercury Molecules

NATIONAL BUREAU OF STANDARDS

The National Bureau of Standards [1] was established by an act of Congress March 3, 1901. The Bureau's overall goal is to strengthen and advance the Nation's science and technology and facilitate their effective application for public benefit. To this end, the Bureau conducts research and provides: (1) a basis for the Nation's physical measurement system, (2) scientific and technological services for industry and government, (3) a technical basis for equity in trade, and (4) technical services to promote public safety. The Bureau consists of the Institute for Basic Standards, the Institute for Materials Research, the Institute for Applied Technology, the Institute for Computer Sciences and Technology, and the Office for Information Programs.

THE INSTITUTE FOR BASIC STANDARDS provides the central basis within the United States of a complete and consistent system of physical measurement; coordinates that system with measurement systems of other nations; and furnishes essential services leading to accurate and uniform physical measurements throughout the Nation's scientific community, industry, and commerce. The Institute consists of a Center for Radiation Research, an Office of Measurement Services and the following divisions:

Applied Mathematics — Electricity — Mechanics — Heat — Optical Physics — Nuclear Sciences [2] — Applied Radiation [2] — Quantum Electronics [3] — Electromagnetics [3] — Time and Frequency [3] — Laboratory Astrophysics [3] — Cryogenics [3].

THE INSTITUTE FOR MATERIALS RESEARCH conducts materials research leading to improved methods of measurement, standards, and data on the properties of well-characterized materials needed by industry, commerce, educational institutions, and Government; provides advisory and research services to other Government agencies; and develops, produces, and distributes standard reference materials. The Institute consists of the Office of Standard Reference Materials and the following divisions:

Analytical Chemistry — Polymers — Metallurgy — Inorganic Materials — Reactor Radiation — Physical Chemistry.

THE INSTITUTE FOR APPLIED TECHNOLOGY provides technical services to promote the use of available technology and to facilitate technological innovation in industry and Government; cooperates with public and private organizations leading to the development of technological standards (including mandatory safety standards), codes and methods of test; and provides technical advice and services to Government agencies upon request. The Institute consists of a Center for Building Technology and the following divisions and offices:

Engineering and Product Standards — Weights and Measures — Invention and Innovation — Product Evaluation Technology — Electronic Technology — Technical Analysis — Measurement Engineering — Structures, Materials, and Life Safety [4] — Building Environment [4] — Technical Evaluation and Application [4] — Fire Technology.

THE INSTITUTE FOR COMPUTER SCIENCES AND TECHNOLOGY conducts research and provides technical services designed to aid Government agencies in improving cost effectiveness in the conduct of their programs through the selection, acquisition, and effective utilization of automatic data processing equipment; and serves as the principal focus within the executive branch for the development of Federal standards for automatic data processing equipment, techniques, and computer languages. The Institute consists of the following divisions:

Computer Services — Systems and Software — Computer Systems Engineering — Information Technology.

THE OFFICE FOR INFORMATION PROGRAMS promotes optimum dissemination and accessibility of scientific information generated within NBS and other agencies of the Federal Government; promotes the development of the National Standard Reference Data System and a system of information analysis centers dealing with the broader aspects of the National Measurement System; provides appropriate services to ensure that the NBS staff has optimum accessibility to the scientific information of the world. The Office consists of the following organizational units:

Office of Standard Reference Data — Office of Information Activities — Office of Technical Publications — Library — Office of International Relations.

---

[1] Headquarters and Laboratories at Gaithersburg, Maryland, unless otherwise noted; mailing address Washington, D.C. 20234.
[2] Part of the Center for Radiation Research.
[3] Located at Boulder, Colorado 80302.
[4] Part of the Center for Building Technology.

Analysis of Optically Excited Mercury Molecules

R. E. Drullinger, M. M. Hessel,
and E. W. Smith

Quantum Electronics Division
Institute for Basic Standards
National Bureau of Standards
Boulder, Colorado 80302

Supported by:

Los Alamos Scientific Laboratory under AEC Order No. LS74-4 and the Advanced Research Projects Agency under ARPA Contract 981, Amendment No. 9.

U.S. DEPARTMENT OF COMMERCE, Frederick B. Dent, *Secretary*

NATIONAL BUREAU OF STANDARDS, Richard W. Roberts, *Director*

Issued January 1975

Library of Congress Cataloging in Publication Data

Drullinger, R. E.
Analysis of Optically Excited Mercury Molecules.

(National Bureau of Standards Monograph; 143)
Supt. of Docs. No.: C 13.44:143
1. Laser Spectroscopy. 2. Mercury—Spectra. 3. Excited State Chemistry. I. Hessel, Merrill M., 1933- joint author. II. Smith, Earl William, 1940- III. Title. IV. Series: United States. National Bureau of Standards. Monograph; 143.
QC100.U556 No. 143 [QD96.L3] 389'.08s [546'663'6] 74-31115

National Bureau of Standards Monograph 143

Nat. Bur. Stand. (U.S.), Monogr. 143, 51 pages (Jan. 1975)

CODEN: NBSMA6

U.S. GOVERNMENT PRINTING OFFICE
WASHINGTON: 1975

For sale by the Superintendent of Documents, U.S. Government Printing Office, Washington, D.C. 20402
(Order by SD Catalog No. C13.44:143).
Price $1.10

CONTENTS

LIST OF FIGURES

Analysis of Optically Excited Mercury Molecules

R. E. Drullinger, M. M. Hessel, and E. W. Smith

The Hg_2 molecule is representative of a class of molecules which have dissociative ground states and bound excited states. It can therefore be used as a prototype of this class of molecules which are of interest as potential new laser candidates. Because of the non-bound ground state, standard absorption spectroscopic techniques cannot be used to obtain the necessary information about the excited states. We have therefore developed new measurement techniques to obtain potential curves, f-values, and kinetic behavior for Hg_2. These techniques are applicable to this whole class of dissociation molecular systems.

Key words: Dissociation laser; excimers; excited state kinetics; f-values; mercury molecules; new spectroscopic techniques; optical excitation; potential curves.

I. INTRODUCTION

There is currently much interest in the development of high energy tunable lasers in the visible and near UV. "Dissociation lasers" operating on electronic transitions in molecules having dissociative ground states give promise of achieving this goal. The molecules of interest as dissociation laser candidates include pure metals such as Hg_2, Zn_2, Cd_2; mixed metals such as HgZn; metal-noble gas molecules such as HgXe, LiXe; and pure noble gas dimers. Research on this class of laser has been impeded because most of the interesting systems include metals which are highly reactive at the high pressures and temperatures of laser interest. Furthermore, the dissociative nature of the electronic ground state severely inhibits conventional absorption spectroscopy hence, even for such ubiquitous systems as Hg_2, there exists very little basic data (eg. A values, potential energy curves, energy transfer rates, etc.). At the present time, only pure rare gas systems have been made to lase, and even these are poorly understood.

The mercury system is currently the most attractive of the metal vapors from the point of view of developing the measurement techniques and gathering the basic data needed for understanding this class of lasers. Some, albeit very little, information is available about molecular mercury from research extending back more than 70 years. The mercury molecule, while somewhat reactive at high temperatures, can still be studied in conventional glass or quartz cells and discharge excitation is also relatively easy to obtain. Previous analyses of electronically excited mercury molecules can be roughly divided into three categories according to the type of excitation employed: (1) optical excitation via the atomic resonance line[1] (253.7)nm at mercury pressures less than 1 torr (1 torr = 133 N/m^2), (2) low pressure discharge excitation[2] and, more recently, (3) high

energy (Mev) electron beam excitation at pressures of several hundred torr or more[3]. Each of these techniques has provided useful information and each has its limitations. Discharge excitation can produce a fairly high density of excimers (electronically excited molecules whose ground state is dissociative) but the analysis of the states of interest is confused by the presence of charged particles and highly excited molecular states which can act as metastable energy reservoirs or as absorbers. Resonance line optical pumping avoids these difficulties (if the resonance lamp is suitably filtered), but this technique is restricted to mercury pressures well below the range of laser interest because, at pressures of 1 torr or more, the exciting radiation is all absorbed in a very thin sheath at the edge of the vapor and interactions with the wall dominating the observations.

In this paper, we report results obtained with a type of optical pumping[4] which is applicable from a few torr to several atmospheres. High power continuum lamps have been used to populate Hg_2 excited states directly from the weak Van der Waals well and continuum region of the electronic ground state. Figure 1.1 shows the postulated Hg_2 potential curves[5] and the location of the absorption band which we have used for our optical pumping (it must be emphasized that very little is known about these curves and figure 1 may be shown to be incorrect by future research. This absorption band was studied extensively by Kuhn and Freudenberg[6] and Lennuier[4] and has been shown to extend from the resonance line at 253.7 to beyond 320 nm depending on the pressure and temperature. The band is optically thick in the region of 253.7 nm but we have produced strong volume excitation even at pressures of 10 atm. The details of this optical pumping technique and the various experimental procedures are discussed in section 2.

In section 3, we present an analysis of steady state data from the 335 and 485 nm fluorescence bands. This analysis indicates that the excited electronic states which emit these bands (and probably the entire manifold of states which arise from $6\ ^3P_J + 6\ ^1S_0$) are in thermal equilibrium among themselves (but <u>not</u> with the electronic ground state). This analysis also gives a 6500 cm^{-1} activation energy for transitions from the 485 reservoir to the 335 reservoir.

In section 4, we present some preliminary time decay data which shows that the 485 and 335 bands decay with the common lifetime and this lifetime is a strong function of the temperature and density of the mercury vapor.

II. EXPERIMENTAL

In this section, we describe the mercury containment cells, filling procedure, oven and temperature controllers, light sources used to excite the molecular spectra, detection systems, spectrographs, and calibration procedures. Purity of the cells and mercury used in these experiments is of the utmost importance; some anomalous results that we obtained by filling the cells with laboratory grade triple-distilled mercury and ordinary vacuum techniques will be discussed along with the mercury handling procedures we have now developed.

In all the experiments described in this monograph, we used a light source to excite mercury vapor contained in a quartz cell. The pressure of the mercury was determined by a cold finger attached to the cell and the temperature was controlled by heating the cell body. Figure 2.1 is a typical schematic of our apparatus.

A. Cell and Oven

The cells were made from 2.5 cm dia. quartz tubing in the form of a cross. The four windows were of UV grade quartz and fused onto the cell body. The optical path length between windows was 3.65 cm. The cell had a small tube extending from its body that acted as a reservoir for the mercury and as a cold finger so that the mercury vapor pressure could be varied independently of cell temperature. Since the cell body was not made out of UV-grade quartz, it fluoresced strongly in a broad band centered around 400 nm if any of the exciting radiation impinged on it. To help eliminate this problem a mask of liquid gold* was painted around the edge of each window to help prevent incident radiation from directly entering the cell body and to mask the fluorescing edge of the cell from the detection optics. Cells of this design could not be operated much above atmospheric pressure (densities $\lesssim 10^{19}\text{cm}^{-3}$).

The cell was contained in a two compartment oven constructed of low density fire brick in which the compartments were heated separately, each with a temperature regulating system. The upper part of the oven where the cell proper was housed determined the mercury vapor temperature and was equipped with four window ports to coincide with the four windows on the cell, each port was fitted with a quartz window to prevent heat loss (see fig. 2.1). Inside this oven and surrounding the cell was a thin-walled stainless steel cylinder with four window ports cut in it. This provided additional heat and light baffling as well as providing a base on which the heater was wound.

The lower oven housed the mercury reservoir and had no windows, thus providing maximum temperature stability and uniformity. Thermocouples were attached directly to the glass side arm at a point where it was full of liquid mercury. The side arm also had a thin layer of asbestos wrapped on it

* A thick organic solution containing gold which when painted on a surface, dried and heated to $> 600^{\circ}\text{C}$ leaves a thin layer of gold bonded to the surface. The usual coating of "aquadag" will not work as it burns off in air at temperatures above 500°C.

and was finally wrapped with several layers of heavy aluminum foil to insure temperature uniformity. The heater for this part of the oven was a coil of nichrome wire wound just on the inside of the fire brick.

Both oven compartments were heated by direct current through series regulators whereby the current to the heater was controlled by the difference potential between the control thermocouple and a reference voltage set to the desired temperature.

This system was of low heat capacity and temperature changes as large as 300°C could be accomplished within 15 minutes. However, tight regulation controlled the reservoir temperature to ± 0.05°C for periods as long as several days resulting in mercury vapor density control to better than 0.5%.

B. Purity Problems and Cell Filling Procedures

In the older literature[7], it had been noted that air and other gases destroyed the fluorescence. More recently Stupavsky, Drake, and Krause[8] observed an anomalous Hg_2 band that Vikis and LeRoy[9] have subsequently suggested was due to an impurity of HgCl. In general, mercury is known[10] to combine with many atomic and molecular species. For these reasons, it is necessary to take great care to insure purity in preparing sample cells.

In our initial experiment, we filled the cells with laboratory grade triple-distilled mercury. The cell was pumped down to a pressure of 10^{-7} torr and baked to 300°C before the Hg was distilled into it. We found that when the cells were heated to give a mercury pressure of 2-5 atm and exposed to any of the blue argon ion laser lines, the characteristic 485 nm blue-green Hg_2 fluorescence band appeared. The first cell failed, however, when the pressure exceeded several atmospheres. With a new cell and slightly improved vacuum techniques, we tried to reproduce and study this laser induced fluorescence effect under carefully controlled conditions. The fluorescence was weaker and lasted only a few hours after initial heating. With the improved vacuum techniques for preparing mercury cells as described below, this laser induced fluorescence completely disappeared, indicating that it is probably produced by an impurity in some laboratory grade mercury. Although time has not allowed an investigation of this "sensitized fluorescence", we have used it as an indication of the cleanliness in the various cells.

The cells used for the experiments described in this monograph were prepared in the following manner:

Prior to the actual filling of a cell, laboratory grade, triple-distilled mercury is distilled into ampules with the arrangement shown in figure 2.2. The ampule filling apparatus is attached through a "U" tube trap to a bakeable vacuum station and the entire system is baked at 400°C for 24 hours. On cooling, a vacuum of $\sim 10^{-9}$ torr is attained. The system is then backfilled with

argon to 1 atm pressure and opened at point A. Laboratory grade mercury is injected into point C and the system closed at point B. The "U" tube trap is then cooled with liquid N_2 and the argon is pumped out of the system. The pressure at this point with the Hg vapor trapped out, is $\simeq 2 \times 10^{-8}$ torr. Using a foam plastic cup fitted over the filling tube (B) and inverted "U" tube (D) and filled with dry ice, a reflux column is set up; C $\rightleftarrows$ B. A small fraction of the refluxing Hg migrates over into the ampules. When an ampule is filled with approximately 5 gm of mercury, it is tipped off and removed from this system. This procedure results in ampules of pure mercury sealed under a vacuum of a few times 10^{-8} torr. To keep the pumping station clean, the remaining system is again filled with argon and cut between the liquid nitrogen trap and the permanent part of the station. This removes all glass that has been exposed to mercury.

To fill a cell, the arrangement shown in figure 2.3 is constructed on the pumping station. It consists simply of the cell to be filled, an ampule of mercury and a "U" tube for a trap. Since the cell is to be operated at temperatures up to 900°C, it must be baked at least to this temperature. For this purpose, a small oven made of a heater and fire brick is placed around the cell inside the main bake-out oven. This allows the cell to be baked out at 1000-1100°C while the rest of the vacuum station is baked at 400°C for 24-36 hours. After the bake-out, the system is cooled, the small oven removed, the trap cooled in liquid nitrogen and the mercury ampule opened. At this point and throughout the rest of the filling procedure, the pressure on the vacuum side of the trap is less than 10^{-8} torr. Some of the mercury is then transferred, again by distillation, into the cell. Mercury often boils violently when distilled and mercury droplets entrained in the vapor could be carried directly into the cell. To prevent this, we boil the mercury gently and make the glass between the Hg ampule and the cell of sufficient length and slope (fig. 2.3) so that any entrained mercury condenses on the walls and rolls back toward the ampule. During the tip-off operation, the cell is heated to cause a large flux of mercury vapor to sweep out past the tip-off point and carry with it out-gassed products of the tip-off operation.

With the cells prepared in this manner and with appropriate excitation, we have been able to observe Hg_2 fluorescence over a density range of 10^{16} to $10^{20} cm^{-3}$ and vapor temperatures of 175 to 800°C. These signals are stable and show no change over 24 hours of operation. With these clean vapors, we do not observe fluorescence induced by any of the Ar^+ laser lines.

C. Optical Pumping and Light Sources

Lennuier[4] and Kuhn and Freudenberg[6] have shown that mercury vapor absorbs radiation in a broad band from the 253.7 nm resonance line to beyond 320 nm. This type of optical pumping is a "clean" technique, in which only the bands of interest (335 and 485 nm) are excited and fluorescence is produced throughout the cell. Figure 2.4 shows Kuhn and Freudenberg's relative absorption coefficient α as a function of wavelength where $I/I_o = e^{-\alpha x}$. Also plotted on the same graph is the ratio R of integrated fluorescence intensity of the 335 band to the exciting wavelength intensity as a function of exciting wavelength at a pressure of 600 torr.[4]

These results show that one can couple power into any depth of mercury vapor and at almost any vapor density and thus obtain volume excitation. To make full use of this pumping scheme for densities up to $10^{20}cm^{-3}$, we have used several types of lamps to maximize the power in the wavelength region effective at the particular density region investigated. At low densities $\lesssim 10^{16}cm^{-3}$ a germicidal resonance lamp is most effective, for densities from 10^{16} to $10^{18}cm^{-3}$ a medium pressure (Osram type) mercury lamp most effectively excites the Hg_2 bands. Above $10^{18}cm^{-3}$ high pressure xenon and mercury-xenon compact arc lamps are used. We recently obtained a commercial ADP frequency doubler which was used to double the 514.5 nm Argon ion laser line thus producing a 10 mW beam of 257.2 nm radiation. This light source produces a small volume, high density excitation.

For the rather preliminary time resolved studies which are presented in section IV, a coaxial system consisting of a 10J energy storage capacitor, a switching thyratron and a 2-4 mm air spark gap was used. During the .5-1 μsec discharge time of the circuit, the air spark radiated light with a spectral distribution roughly corresponding to a 10,000 K blackbody.

Each of these light sources (except for the laser) was used in conjunction with an optical system which collected, collimated, filtered and refocused the light into the cell. This system consists of simple,single element f/1.5 quartz lenses and a tri-compartmented cell which contained the desired combination of filter solutions, see figure 2.1. The filter used throughout most of this work is one of $NiSO_4$-H_2O, $CoSO_4$-H_2O and pure Cl_2 gas. This combination gives a high transmission ($T_{max} > 50\%$) at 270 nm; the transmission curve is given in figure 2.5.

In addition to the light sources above, we have used the 337.1 nm output of a pulsed 1 MW nitrogen laser to excite the mercury vapor. The 485 nm band fluorescence was observed through a broad band 480 nm interference filter at densities in excess of $10^{19}cm^{-3}$. A cw He-Cd laser (10 mW at 325 nm) also excites the Hg_2 band fluorescence at densities $> 10^{19}cm^{-3}$. In both cases the excitation was rather weak and neither technique was used beyond the initial trials.

D. Detection Systems

To detect the molecular mercury bands at 335 and 485 nm we have used both S(Q) blue response and S-20 red response photomultipliers. To observe the molecular bands in the appropriate spectral region we either used the photomultipliers with filters or a 1/3 meter scanning monochrometer, depending on the type of experiment and light intensity. The transmission curves of the broadband interference filters used to measure the 335 and 485 band, are shown in figures 2.6 and 2.7.

The spectrometer was calibrated for wavelength, instrument line profile, and (with each of the photomultipliers) quantum efficiency. The spectrometer has a spectral line width of 0.07 nm (FWHM) at a slit width of 10 μm and a line width of 0.3 nm at a slit width of 135 μm. The spectrometer scattered light level beyond 1.5 band widths was found to be < 0.5% in both cases. We generally used slit widths corresponding to an instrumental bandwidth of 0.3 - 1.0 nm. We used a spectral irradiance tungsten iodine lamp[11] to calibrate the photomultiplier and spectrometer combinations for relative quantum efficiency. The lamp was essentially a blackbody source at a specific color temperature for a fixed current input to the lamp. In our case, the calibration was made at two color temperatures 3110 ± 15 K and 2785 ± 15 K. The independent calibrations agreed to within ± 1% in the spectral region 300-700 nm.

III. STEADY STATE DATA

A. Band Shapes

The cw-optical pumping schemes described in the previous section have been used to excite mercury vapor at pressures ranging from about one torr to several atmospheres and temperatures ranging from 175°C to 1000°C. The entire fluorescence spectrum has been scanned under moderate resolution (about 0.3 nm to 1.0 nm) from 230 nm to 700 nm using various spectrometers and photomultipliers. A typical photoelectric trace is shown in figure 3.1. This trace was taken with a 1/3 meter spectrometer, with a resolution of about 0.3 nm, using a photomultiplier with an S(Q) response curve. The total response of the instrument was calibrated using a standard lamp, and the trace shown in figure 3.1 includes this correction factor. (The intensities reported in this paper are proportional to the number of photons per wavelength interval.) Since the correction factor with the S(Q) phototube becomes rather large for $\lambda > 550$ nm, another trace was made using the same spectrometer with an S-20 phototube. This particular curve shows fluorescence excited with the 150 W Xe continuum lamp filtered to pass only 240 to 290 nm radiation (discussed in Section II). Since this is a very high intensity source, the radiation scattered by the cell constitutes an appreciable signal which is seen in figure 3.1 as a continuum between 240 and 290 nm. Measurements of this scattering, taken with the cell at room temperature, enable us to subtract out its contribution but it doesn't interfere appreciably with the 335 band in any case.

A similar curve, excited with the frequency doubled Argon ion laser, is shown in figure 3.2. In this case, the doubled laser output was focused into a small volume thus creating a high excimer density (estimated at $10^{13}/cm^3$) and some secondary pumping of the 7^3S_1 state of atomic mercury is observed. This figure also shows scattering of the doubled laser line at 257.2 nm as well as a small amount of the primary laser line at 514.5 nm which scattered into the cell. More recent runs using unfocused 257.2 excitation show no atomic emission and with better filtering, the 514.5 scatter has been removed. Comparison of laser excited fluorescence data with lamp excited data shows no difference between the two (other than a weak excitation of the 7^3S_1 obtained by focusing the laser into a small volume).

It is interesting to note that the peak of the familiar 485 band occurs at 510 nm in figures 3.1 and 3.2. In our uncorrected traces the peak occurred at 485 but when the data are corrected for the spectrometer response function, the true maximum appears at 510. The 335 band shape is essentially unchanged when corrected for the spectrometer response function. Since the band shapes and the location of the maximum intensity are rather important quantities in evaluating potential curves and transition probabilities, the shift of the apparent maximum from 485 nm to 510 nm emphasizes the need for well-calibrated detection systems.

The shapes of the 335 and 485 bands as functions of density and temperature are shown in figures 3.3 - 3.6. The integrated band intensities are normalized to unity in order to show the shifts of the populations within the respective bands. As temperature is increased, both bands show a decrease in peak intensity, an overall broadening of the band and a slight shift toward the blue. This is what one would expect from a Boltzmann distribution of vibrational states; that is, an increase in temperature reduces the population at the bottom of the well which radiates the intensity maximum, and correspondingly increases the population of the higher vibration states which radiate in the wings of the band. The shift to the blue will be discussed later in this section.

Figures 3.5 and 3.6 show that the band shapes are not affected by changes in density. This is also what one would expect from a thermal distribution of vibrational states since the Boltzmann factor is independent of density. The absence of density dependence of the shape of the 485 band cannot be used to confirm or deny the mechanism of collision induced radiation which is often proposed for this band.

B. Band Intensities

The intensities of the 485 and 335 bands were measured as functions of temperature and density. Most of these measurements were made using filters in front of a photomultiplier rather than a spectrometer in order to increase the signal and thereby extend the range of these measurements. A comparison of the filter functions, figures 2.6 and 2.7, with the observed spectral distribution, figure 3.1, shows that the filters did not integrate the entire band. The filters do cover the center of the bands hence the readings are proportional to the total band intensities and the intensity ratios should be accurate. This assertion was checked by integrating spectrometer tracings, such as figure 3.1 in the temperature-density range where spectrometer measurements could be made; the intensity ratios obtained with the filters agreed with those obtained from spectrometer tracings to better than 1%. We certainly do not propose this figure as an estimate of the error in all of our data, but it does nonetheless indicate excellent agreement between these two measurement techniques at least as far as intensity ratios are concerned.

In figure 3.7, we have plotted the log of the intensity ratio R = I(485)/I(335) versus 1/kT where kT is in cm^{-1}. Figure 3.7 shows only six representative curves but several sets of similar data have been analyzed by computer. A linear least squares program was used to fit the data points for $N > 10^{17}$ and $T > 575$ K (i.e. $1/kT < 2.5 \times 10^{-3}$). The slopes in the linear portion of the data, (solid lines) $T \geq 573$ K, give an activation energy of 6500 cm^{-1} with a ± 2% scatter and this scatter appears random; that is, there is no systematic trend in the calculated slope as a function of density. This linearity shows that, for $T \geq 575^{o}K$ and $N > 10^{17}$, the populations are related by

$$N_{335}/N_{485} \propto e^{-\varepsilon/kT} \qquad (3.1)$$

where $\varepsilon = 6500\ cm^{-1}$ to within ± 2%. The fact that there is no variation in this slope over nearly two orders of magnitude in density provides a compelling argument that the two electronic states (which radiate 485 and 335 respectively) are in thermal equilibrium.

The $N = 10^{17}$ run was not analyzed by computer because there are not enough points at high temperatures to be certain about where thermal equilibrium applies. A straight line was drawn through these data with a $6500\ cm^{-1}$ slope for comparison with the other data. The $N = 5 \times 10^{16}$ run clearly shows that the two electronic states are not in equilibrium with one another at this density.

The deviation observed by decreasing the temperature at a constant density is not the only means of achieving a deviation from equilibrium. Another technique is to lower the density for a fixed temperature. This is illustrated in figure 3.8 where we plot the intensity ratio R versus density for several fixed temperatures lying both above and below the critical value of 575 K discussed above. In addition to our data, we have also plotted some low density data of Matland and McCoubrey[12] which were obtained with the resonance line excitation discussed in Section I. It should be noted that the latter were taken in the afterglow (after switching off their resonance lamp) whereas our data are taken in steady state with a continuum lamp. Since the two electronic states are not in thermal equilibrium for $N < 10^{17}$, this may not be a valid comparison. None of the data in this figure have been calibrated to account for the band width of the filters or the relative sensitivity of the phototube in the blue 335 and green 485 regions. These corrections would only multiply R by a constant, hence the slope of the curves is correct even though the vertical position of the curves is arbitrary. That is, the fact that our data at 470 K joins smoothly with the Matland-McCoubrey data at 473 K is fortuitous. Furthermore, the 519 K curve lies above the 470°K only because it was arbitrarily displaced upward one order of magnitude to make the data easier to read, the actual measurements lie between the 470 K and 623 K curves. The two asymptotes $R \propto N^2$ and $R \propto N$ have been drawn in as dashed lines to aid in the interpretation of the data.

We first consider the region $N > 10^{17}$ on the 631 K and 623 K curves. The previous discussion has shown that the states radiating 485 and 335 are in thermal equilibrium for this temperature-density range, yet figure 3.8 shows that the intensity ratio increases linearly with N over at least two decades in N. Assuming that the 335 nm radiation is due to spontaneous emission, this would indicate that 485 is radiated either by the collision induced mechanism

$$Hg_2^* + Hg \rightarrow 3Hg + h\nu_{485} \tag{3.2}$$

or by stable Hg_3^*:

$$Hg_2^* + Hg \rightarrow Hg_3^* \tag{3.3}$$

$$Hg_3^* \rightarrow 3Hg + h\nu_{485} \tag{3.4}$$

It is impossible to distinguish between these two mechanisms with our current data.

We next consider the data for $N < 10^{17}$. These data show a strong tendency toward an N^2 dependence at the lower densities. Although none of these data are truly parallel to the N^2 asymptote, they seem to be approaching it more closely as N decreases. The transition from N^2 to N dependence seems to occur at about 10^{17}. This change is rather difficult to detect in the 623 K data but there are clear systematic deviations from linearity for the low density points on this curve. It would be desirable to have more points at lower N for this temperature because this is one of the cases which is clearly in thermal equilibrium when $N > 10^{17}$. It would therefore be instructive to measure more accurately its deviation from the linear N dependence as N is decreased. Unfortunately, the 485 band becomes very weak for low N and high T and it was possible to go to lower N only for the lowest temperatures (such as the 519 K curve for example). The latter overlaps the 10^{17} region very well; this curve agrees quite well with the low pressure afterglow measurements of Matland-McCoubrey[12] but at high N it never quite achieves the linear N dependence exhibited by the high temperature data. This is not surprising since, in view of figure 3.7 we would not expect to be in thermal equilibrium at this temperature.

In summary then, we have compelling evidence that the states responsible for the 485 and 335 fluorescence band are in thermal equilibrium for high temperatures $T \gtrsim 575$ K and densities $N \gtrsim 10^{17}$. In the high temperature-density region where thermal equilibrium applies, the linear dependence of R = I(485)/I(335) on N would seem to indicate that 485 is emitted by a density dependent process such as collision induced radiation, eq. (3.3), or Hg_3^* formation, eqs. (3.4) and (3.5).

C. Potential Curves

In this section, we present a preliminary analysis of the electronic potential curves involved in the 485 and 335 fluorescence. For similar discussions see Hedges, et. al. [13], Doyle[14] or Sando and Dalgarno[15]. The number of photons per unit wavelength emitted in a transition between a bound excited electronic state "a" and a repulsive ground state "b" is

$$I_\lambda = \frac{CN^*(T)}{\lambda^5} \Sigma_{vJJ'} \int d\epsilon\ \delta(h\nu - E_{avJ} + \epsilon)$$

$$= \frac{\exp(-E_{avJ}/kT) S_{JJ'}}{Z(T)} \left| D_{avJ,b\epsilon J'} \right|^2 \qquad (3.5)$$

$$\times \frac{CN^*(T)}{\lambda^5} \Sigma_{vJJ'} \frac{\exp(-E_{avJ}/kT) S_{JJ'}}{Z(T)} \left| D_{avJ,b\epsilon J'} \right|^2$$

where (v,J) are vibration rotation quantum numbers for a, (ϵJ') are the corresponding quantum numbers

for b (ε is a continuous nuclear kinetic energy quantum number), D is the transition dipole moment, S is the Honl-London factor, the total number of excimers is $N^*(T)$, the excimer state population densities are described by a Boltzmann distribution with a partition function Z(T), and C denotes miscellaneous uninteresting constants. The integral over nuclear kinetic energy ε removes the delta function and, in the second line, ε equals $(E_{avJ}-h\nu)$.

The dipole matrix element in eq. (3.5) can be expressed in terms of vibrational wavefunctions as

$$D_{avJ,b\varepsilon J'} = \int_0^\infty D_{ab}(R)\Psi^J_{av}(R)\Psi^{J'}_{b\varepsilon}(R)dR \tag{3.6}$$

where $D_{ab}(R)$ denotes the dipole matrix element between the electronic states a and b. This integral can be evaluated using WKB wavefunctions[16] in which case one finds that the integrand is sharply peaked about a critical radius R_λ at which the radial momenta for upper and lower states are equal (Franck-Condon principle):

$$\sqrt{\varepsilon - V_b(R_\lambda) - \frac{\hbar^2 J'(J'+1)}{2\mu R_\lambda^2}} = \sqrt{E_{avJ} - V_a(R_\lambda) - \frac{\hbar^2 J(J+1)}{2\mu R_\lambda^2}} \tag{3.7}$$

or since, $\varepsilon = E_{avJ}-h\nu$,

$$\begin{aligned} h\nu &= V_a(R_\lambda) - \frac{\hbar^2 J(J+1)}{2\mu R_\lambda^2} - V_b(R_\lambda) - \frac{\hbar^2 J'(J'+1)}{2\mu R_\lambda^2} \\ &\simeq V_a(R_\lambda) - V_b(R_\lambda) \end{aligned} \tag{3.8}$$

In the last line of eq. (3.8) we have used the fact that the rotational levels with large thermal populations correspond to large J values, thus the $\Delta J = \pm 1,0$ selection rule implies that the rotational energies in eq. (3.8) essentially cancel out. That is, for a given vibrational level and a specific R_λ, all rotational levels emit photons of essentially the same frequency. There is some rotational broadening due to the inexact cancellation of the rotational energies, but this is negligible for our purposes. Since the integrand in Eq. (3.6) is sharply peaked at R_λ, the function D_{ab} may be factored out as $D_{ab}(R_\lambda)$ and the remaining Franck-Condon overlap integral evaluated by the method of stationary phase. Mies[16] argues that the WKB phase integral (the integral over the radial momentum) for the repulsive state b will be small (compared with π) at the point R_λ. Equation (3.6) then reduces to

$$D_{avJ,b\varepsilon J'} = D_{ab}(R_\lambda)\Psi^J_{av}(R_\lambda)\left[\left(\frac{\hbar^2}{2\mu}\right)\frac{d}{dR_\lambda}\left\{V_a(R_\lambda) - V_b(R_\lambda)\right\}\right]^{-1} \tag{3.9}$$

If the WKB phase integral is not small Ψ^J_{av} is replaced by a slightly more complicated function of R_λ. We must therefore emphasize that, for the high temperatures of interest to us ($T \gtrsim 400$ K) this phase integral will be small only if R_λ lies near the classical turning point for the repulsive state

(within 0.5 Å). This will be a good approximation since the WKB continuum wavefunction is sharply peaked about the classical turning point. In fact, one must be somewhat careful about using a WKB wavefunction for $\Psi^J_{av}(R_\lambda)$ because the latter diverges at the turning point. However, eq. (3.9) can also be derived using Airy wavefunctions which do not diverge[17], hence one can readily find well behaved wavefunctions for use with this expression. It should be noted that eq.(3.9) is quite similar to the "reflection method"[18] in which the repulsive state wavefunction is replaced by a delta function at the classical turning point. It should also be noted that eq. (3.9) breaks down if the derivative of $(V_a - V_b)$ should vanish at R_λ; in such a case one must use the full Airy function results[17] (i.e. without assuming that the WKB phase integral for state b is small).

We next note that the vibrational wavefunction Ψ^J_{av} depends on J only through the radial kinetic energy $E_{avJ} - V_a(R) - \hbar^2 J(J+1)/2\mu R^2$. Since for not too large values of J the shape of the potential energy curve $V_a(R) + \hbar^2 J(J+1)/2\mu R^2$ does not differ appreciably from that of $V_a(R)$, we will approximate the rotational energy by $\hbar^2 J(J+1)/2\mu R_\lambda^2$. This approximation ignores a small distortion produced by the rotational energy but this should be negligible for our purposes[19]. We may therefore replace E_{avJ} in eq. (3.5) by:

$$E_{avJ} = E_{av} - \frac{\hbar^2 J(J+1)}{2\mu R_\lambda^2} \tag{3.10}$$

thus removing all J dependence from the vibrational wavefunction. Substituting eqs. (3.7) and (3.10) into eq. (3.5) and performing the J' sum of $S_{JJ'}$, (which yields (2J + 1)), we obtain:

$$I_\lambda = \frac{CN^*(T)}{\lambda^5} \Sigma_{vJ} \frac{|D_{ab}(R_\lambda)|^2 |\Psi_{av}(R_\lambda)|^2}{(d\nu/dR_\lambda)} \times \frac{(2J+1)\exp\left\{-(E_{av} + \hbar^2 J(J+1)/2\mu R_\lambda^2)/kT\right\}}{Z(T)} \tag{3.11}$$

where Ψ_{av} denotes the (rotationless) vibrational wavefunction with energy eigenvalue E_{av} and the derivative of $(V_a - V_b)$ was replaced by $(d\nu/dR_\lambda)$ according to eq. (3.8). Next using the identity $E_{av} = T_v(R_\lambda) + V(R_\lambda)$ where $T(R_\lambda)$ is the nuclear kinetic energy at the point R_λ and assuming that the rotational spacing is much smaller than kT, we replace the sum over J by an integral which yields

$$I_\lambda = \frac{CN^*(T)}{\lambda^5} \frac{2\mu kT}{\hbar^2} \frac{R_\lambda^2 \exp\left\{-V_a(R_\lambda)/kT\right\}}{(d\nu/dR_\lambda)} |D_{ab}(R_\lambda)|^2 \times \Sigma_v |\Psi_{av}(R_\lambda)|^2 \frac{\exp\left\{-T_v(R_\lambda)/kT\right\}}{Z(T)} \tag{3.12}$$

We have now obtained an expression which relates I_λ to the dipole strength $|D_{ab}(R_\lambda)|^2$ and the probability of finding the nuclei at the radial separation R_λ where the radiative transition takes place. The probability is described by a Boltzmann spatial distribution, $4\pi R_\lambda^2 \exp\{-V_a(R_\lambda)/kT\}$, multiplied by a momentum distribution which is in the form of a sum over vibrational states. Assuming that the vibrational spacing (estimated to be the order of 150 cm^{-1}) is much less than kT (so that many vibrational levels are populated), the sum over vibrational states is easily performed using either harmonic oscillator or WKB eigenfunctions and one obtains $2\mu kT/\hbar^2$. The partition function, which includes both bound and free states, is dominated by the continuum contribution hence,

$$Z(T) \simeq (2\pi\mu kT/\hbar^2)^{3/2} V \tag{3.13}$$

where V is the volume of the system. Defining the density of excited states by $n^*(T)$ we finally obtain (cf. eq. (8) of ref. (13))

$$I_\lambda = Cn^*(T) \frac{R_\lambda^2 \exp\left\{-V_a(R_\lambda)/kT\right\} |D_{ab}(R_\lambda)|^2}{\lambda^5 (d\nu/dR_\lambda)} \tag{3.14}$$

If the temperature is less than or comparable to the vibrational spacing it is better to use eq. (3.12). For our data, eq. (3.14) should be sufficient and it is this expression which we will use to analyze the data presented in this report. For the purposes of our analysis this result can be summarized by writing

$$I_\lambda = \frac{Cn^*(T)}{\lambda^5} f(R_\lambda) \exp\left\{-V_a(R_\lambda)/kT\right\} \tag{3.15}$$

where $f(R_\lambda)$ represents the effective transition probability at the point R_λ.

To use eq. (3.15) effectively, we first consider the ratio of intensities at two different wavelengths in the same electronic band system. The log of this ratio will be (notice that the $n^*(T)$ cancels out)

$$\log(I_\lambda/I_{\lambda'}) = -\left\{\frac{V_a(R_\lambda) - V_a(R_{\lambda'})}{kT}\right\} + \left\{\log \frac{f(R_\lambda)}{f(R_{\lambda'})}\left(\frac{\lambda'}{\lambda}\right)^5\right\} \tag{3.16}$$

If we plot this log versus 1/kT, the slope of the linear plot will give $V_a(R_\lambda) - V_a(R_{\lambda'})$. By doing this for several values of λ', we can plot out V_a as a function of wavelength. Of course, we can't get the absolute energy without using some known energy level as a reference thus, for the present, we will plot V_a relative to some arbitrarily chosen reference point. For convenience, we will choose the energy level which is responsible for 500 nm emission since we always have a strong signal at this wavelength. Figure (3.9) shows a semilog plot of (I_λ/I_{500}) versus 1/kT for several wavelengths in the 485 band; the number in parentheses gives the slope in cm^{-1}. The excellent linearity of these plots shows that the vibrational states are in thermal equilibrium as one would expect. These data, and several more sets, which we have not plotted, have been analyzed by a least squares computer program to obtain the slopes. The resulting $V_a(R_\lambda)$ is plotted in figure (3.10)

together with the ground state curve obtained from the relation $V_b(R_\lambda) = V_a(R_\lambda) - h\nu$. If the 485 band is emitted by Hg_3, our picture of these potential curves figure (3.10), is somewhat altered by the fact that V then depends on two radial parameters as well as the angles between the internuclear vectors.

In figure (3.11) the same procedure has been followed for the 335 band choosing the state which radiates at 336 nm as our energy origin. In figure (3.12), we have plotted I_{336}/I_{500} so that the potential curves for the 335 band can be plotted relative to the energy of the state which radiates at 500 nm. These curves are given in figure (3.13).

At this point, we should emphasize that the potential curves plotted in figures (3.10) and (3.13) were obtained from the slope of the log R versus 1/kT plots in figures (3.9), (3.11) and (3.12). These potentials are therefore unaffected by temperature independent quantities such as f-values, etc.

Figures (3.10) and (3.13) verify the bound-free nature of the 485 and 335 bands. These figures also appear to indicate that the region of the ground state involved in the 485 band lies somewhat higher on the repulsive wall than the region corresponding to the 335 band and there is some overlap at the edges of the bands. This is consistent with figure (1.1) but it does not prove that figure (1.1) is the correct picture because we only have V versus λ not V versus R and one cannot say with certainty that the ground state curves in figures (3.10) and (3.13) actually refer to the same state (e.g. the ground state of Hg_3 is probably similar but not identical to that for Hg_2).

In conclusion we must emphasize that the potential curves V vs λ, presented in this report, are preliminary data and may be somewhat in error, particularly around 350 nm to 400 nm where the fluorescence bands overlap. We are currently taking more extensive data at various pressures which will be computer analyzed to provide greater accuracy.

D. The Effective Transition Probability

It is well known that the probability for emission depends on the internuclear spearation. In eq. (3.14) there are several factors which determine this probability and, in eq. (3.15), we have divided them into two categories according to their temperature dependence. The potential energy $V(R_\lambda)$ and the Boltzmann factor were discussed in the previous section; in this section we will briefly discuss the temperature independent quantity $f(R_\lambda)$.

The function $f(R_\lambda)$ is strongly influenced by the dimensional factor R_λ^2 which (for our case) causes f to increase with decreasing wavelength. Since f is inversely proportional to $(d\nu/dR) \propto (dV_a/dR) - (dV_b/dR)$, this factor will tend to make f larger in the region where both V_a and V_b are repulsive (longer wavelengths) thus counteracting the effect of R^2 to some extent. Finally there is the dipole strength $D_{ab}(R_\lambda)$ where radial dependence is unknown.

It is possible to obtain relative values of f as a function of wavelength by comparing the quantity

$$I'_\lambda = \lambda^{-5} \exp \{ - V_a(R_\lambda)/kT \} \tag{3.17}$$

with the observed intensity I_λ for some fixed temperature. Such a comparison has been made for both bands and the results are given in tables (3.1) and (3.2). The comparison was made for two different temperatures in order to give an idea of the scatter in calculated values of f. This scatter seems to be the order of 10%, but it should be possible to do a bit better when more accurate potentials are obtained. The functions $f(R_\lambda)$ are relatively constant near the centers of the bands with a rapid increase in the short wavelength (large R_λ) limit.

At this point, no attempt has been made to estimate an absolute value of $f(R_\lambda)$; the present analysis is intended only to give an idea of the type of gain profiles to be expected for these bands.

The blue shift of the peaks of both bands, which was observed with increasing temperature, (figs. 3.3 and 3.4) is now seen to result from a combination of $f(R_\lambda)$ and the λ^{-5} factor in eq. (3.15). These factors combine to make an effective transition probability which increases strongly with decreasing wavelength.

IV. TIME DEPENDENCE

Using the pulsed discharge continuum lamp described in section II C, we have observed the time evolution of the 335 and 485 bands throughout a density range of 10^{17} to 10^{19} Hg atoms/cm^3 and a temperature range of 473 to 973 K. Light from the lamp passed through the tri-compartmental filter (see fig. 2.1) and the resulting fluorescence was observed at right angles through either the 335 or 485 broad band interference filters (fig. 2.6).

Figure (4.1) shows a typical time history trace for a density of 10^{18} and a vapor temperature of 523 K. Part "a" shows the overall rise and decay of the 485 band time with a 10 μsec/div time scale while part "b" shows the rise of the fluorescence with an expanded scale of 2 μsec/div. At low pressures (3×10^{17} cm^{-3}) the rise of the 335 band is the order of 30 μsec and about 25% faster than that of the 485 band, whereas at higher pressures (10^{18}-10^{19} cm^{-3}), the two bands rise almost simultaneously with rise times in the range 10 to 1 μsec. The observed rise times decrease linearly with increasing density but show almost no temperature dependence; increasing only slightly as the temperature increases from 200°C to 350°C and remaining constant after that.

It is interesting to note that while the duration of the flashlamp pulse is 1 μsec., the rise time of the fluorescence bands has been observed to be as long as 40 μsec (at $N = 3 \times 10^{17}$). One possible explanation for this delay assumes that the postulated merging[4] of the $^3\Pi_u$ and $^3O_u^-$ curves (see fig. 1.1) causes the high lying $^3\Pi_u$ vibrational states (which are the ones being directly pumped) to dissociate before they can radiate (the A value is expected to be the order of 10^6 - 10^7) or before collisions can produce vibrational relaxation. The $^3P_0$ atomic state would then serve as a reservoir for this excitation and the slow rise in fluorescence intensity would be determined by the rate at which $^3P_0$ feeds energy back to the molecules. Initial attempts to test this hypothesis by measuring the time history of the $^3P_0$ have been hampered by lack of intensity.

The long time decay fits an exponential, $e^{-t/\tau}$, from 80% of the maximum intensity out to about 3 time constants (the limit of our measurement). Both bands decay simultaneously to within the experiment error of ± 1 μsec at all pressures and temperatures for which we have made the measurement. As shown in figure (4.2) there is a striking temperature dependence; first a sharp increase in lifetime and then a decrease. The point at which the maximum time constant is observed is where the dominant emission changes (see fig. 4.3) from 485 nm (low temperature) to 335 nm (at high temperatures). For a density of 2×10^{18} cm^{-3}, this point is at $T \simeq 730$ K.

The complex behavior of both rise and decay processes indicates the presence of several competing processes. We made several attempts to model the data but more extensive data will be needed before any meaningful analysis is possible.

V. SUMMARY

This report presents new measurement techniques which have been developed to provide data such as potential curves and f-values for metal molecules which are of interest as dissociation laser candidates. Preliminary data and analysis were presented in order to illustrate the measurement techniques in general and to shed some light on the mercury molecule in particular.

Our results may be briefly summarized as follows:

(1) Purity is extremely important. Normal laboratory grade mercury was not pure enough and it was necessary to distill the mercury into specially prepared sample cells.

(2) The two electronic states responsible for the 485 and 335 bands have been shown to be vibrationally equilibrated at the pressures of interest in laser applications.

(3) Assuming that these fluorescence bands are emitted by diatomic mercury, the potential curves for these states have been measured over the regions which give rise to the fluorescence and are found to be in qualitative agreement with curves proposed by Mrozowski. Our results do not extend to large internuclear distances so it is not possible to say if they will agree with Mrozowski in the dissociation limit. However, on the basis of the present data, one cannot exclude the possibility that the 485 band is radiated by Hg_3.

(4) The two electronic states radiating 485 and 335 appear to be in thermal equilibrium with one another, perhaps indicating a curve crossing as proposed by Mrozowski.

(5) Relative transition probabilities were found to be slowly varying across both bands with some increase at larger R or smaller wavelengths.

(6) The pressure and temperature dependence of both decay and rise times have been measured, but no quantitative conclusions have been drawn from these data as yet.

VI. ACKNOWLEDGMENTS

We would like to acknowledge many helpful discussions with Dr. A. V. Phelps and Prof. J. Cooper of the Joint Institute for Laboratory Astrophysics. We also wish to thank Mme. Denise Perrin of the University of Paris VI for providing us with information on the optical pumping of Hg_2 via the continuum absorption band. In addition, we wish to express appreciation to Dr. R. J. Carbone for many stimulating discussions and for organizing a symposium on mercury at the AEC Los Alamos Laboratories which provided many new ideas on the kinetics of such systems.

VII. REFERENCES

1. A. O. McCoubrey, Phys. Rev. 93, 1249 (1954); R. A. Phaneuf, J. Skonieczny, and L. Krause, Phys. Rev. A8, 2980 (1973); J. Skonieczny and L. Krause, Phys. Rev. A9, 1612 (1974) and references contained therein.
2. A. Atajew, A. Rutscher, and R. Winkler, Beit. Plasma Physik 12, 339 (1972); R. J. Carbone and M. M. Litvak, J. Appl. Phys. 39, 2413 (1968); H. Takeyama, J. Sci. Hiroshima Univ. 15, 235 (1952).
3. D. J. Eckstrom, R. M. Hill, D. C. Lorentz, and H. H. Nakano, Chem. Phys. Lett. 23, 112 (1973); R. M. Hill, D. J. Eckstrom, D. C. Lorentz, and H. H. Nakano, Appl. Phys. Lett. 23, 373 (1973).
4. Subsequent to our work, Mme. D. Perrin referred us to the work of R. Lennuier on non resonance line pumping of Hg_2. (a) R. Lennuier, Compt. Rend. 213, 169 (1941), (b) R. Lennuier and Y. Crenn, Compt. Rend. 216, 486 (1943), and (c) R. Lennuier and Y. Crenn, Compt. Rend. 216, 533 (1943).
5. S. Mrozowski, Rev. Mod. Phys. 16, 153 (1944).
6. H. Kuhn and K. Freudenberg, Z. Physik, 76, 38 (1932). Translated by K-B. Persson and M. M. Hessel. A copy of this translation is available upon request to the authors of this report.
7. R. W. Wood, Physical Optics (Dover Publications, Inc. New York) 1961 p. 636.
8. M. Stupavsky, G. W. F. Drake and L. Krause, Phys. Lett. 39A, 394 (1972).
9. A. C. Vikis and D. J. LeRoy, Phys. Lett. 44A, 325 (1973).
10. P. Pringsheim, Fluorescence and Phosphorescence (Interscience, New York, 1949).
11. R. Stair, W. E. Schneider, J. K. Jackson, Appl. Optics 2, 1151 (1963).
12. C. G. Matland and A. O. McCoubrey , unpublished research memo.
13. R. E. M. Hedges, D. L. Drummond, and A. Gallagher, Phys. Rev. 6, 1519 (1972).
14. Robert O. Doyle, J. Quant. Spectrosc. and Radiat. Transfer, 8, 1555, (1968).
15. K. M. Sando and A. Dalgarno , Mol. Phys. 20, 103 (1971).
16. F. H. Mies , J. Chem. Phys. 48, 482 (1968).
17. W. H. Miller , J. Chem. Phys. 48, 464 (1968).
18. G. Herzberg, "Spectra of Diatomic Molecules" Van Nostrand Reinhold Co. 1950, p. 392.

Table 3.1 f_λ for 335 nm band, T = 873K, kT = 605 cm^{-1}

λ	$e^{-(V_\lambda - V_{336})/kT}$	$(\lambda/336)^{-5}\, e^{-(V_\lambda - V_{336})/kT}$	I_{obs}	f
300	0.034	.059	.145	2.46
310	.173	.259	.353	1.36
320	.45	.574	.68	1.18
330	.78	.85	.96	1.12
336	1.0	1.0	1.0	1.0
340	1.02	.96	.93	.97
350	.88	.72	.545	.76
360	.396	.28	.17	.61
	T = 673 K, kT = 467 cm^{-1}			
300	.013	.022	.066	3.0
310	.10	.15	.21	1.4
320	.36	.46	.53	1.15
330	.726	.79	.91	1.15
336	1.0	1.0	1.0	1.0
340	1.03	.97	.97	1.0
350	.85	.69	.55	.8
360	.30	.21	.26 $\pm$ 0.1	1.24

Table 3.2 f_λ for 500 nm band, T = 573 K, kT = 398 cm^{-1}

λ	$e^{-(V_\lambda - V_{500})/kT}$	$(\lambda/500)^{-5}\, e^{-(V_\lambda - V_{500})/kT}$	I_{obs}	f
400	0.00164	.005	.075	11.4
420	.013	.031	.129	4.16
440	.095	.18	.29	1.6
460	.266	.404	.56	1.39
480	.534	.655	.85	1.3
500	1.0	1.0	1.0	1.0
520	1.386	1.14	.96	.84
540	1.05	.715	.765	1.07
560	.78	.44	.52	1.18
580	.405	.193	.32	1.64
	T = 773 K, kT = 536.4 cm^{-1}			
400	0.0086	.026	.289	11.1
420	.041	.098	.388	4.0
440	.174	.33	.562	.17
460	.374	.57	.796	1.4
480	.627	.77	.95	1.23
500	1.0	1.0	1.0	1.0
520	1.27	1.04	.90	.87
540	1.03	.70	.69	.99
560	.83	.47	.51	1.08
580	.51	.243	.33	1.4

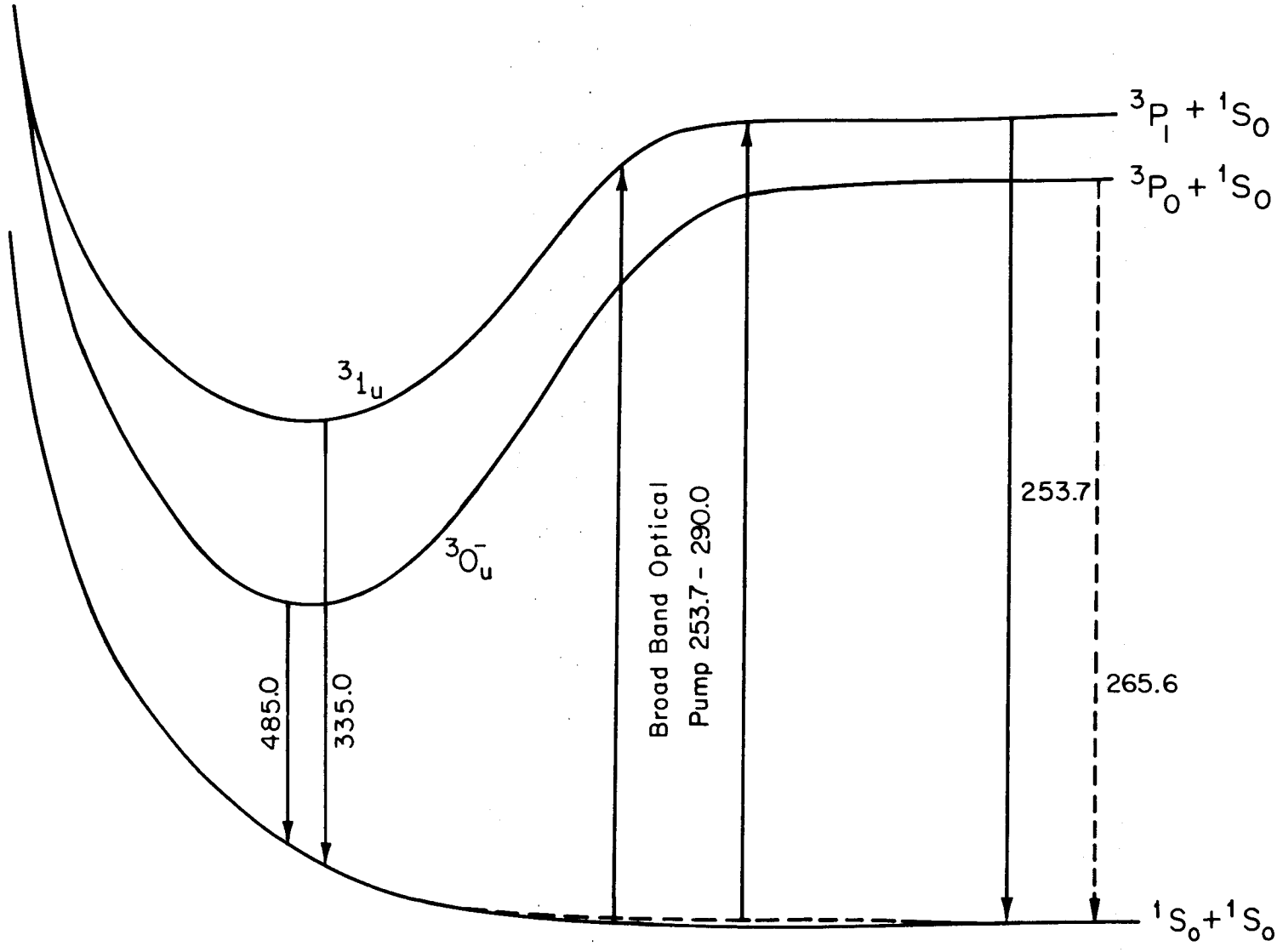

Figure 1.1 Potential curves of Hg_2 molecules according to Mrozowski (ref. 5).

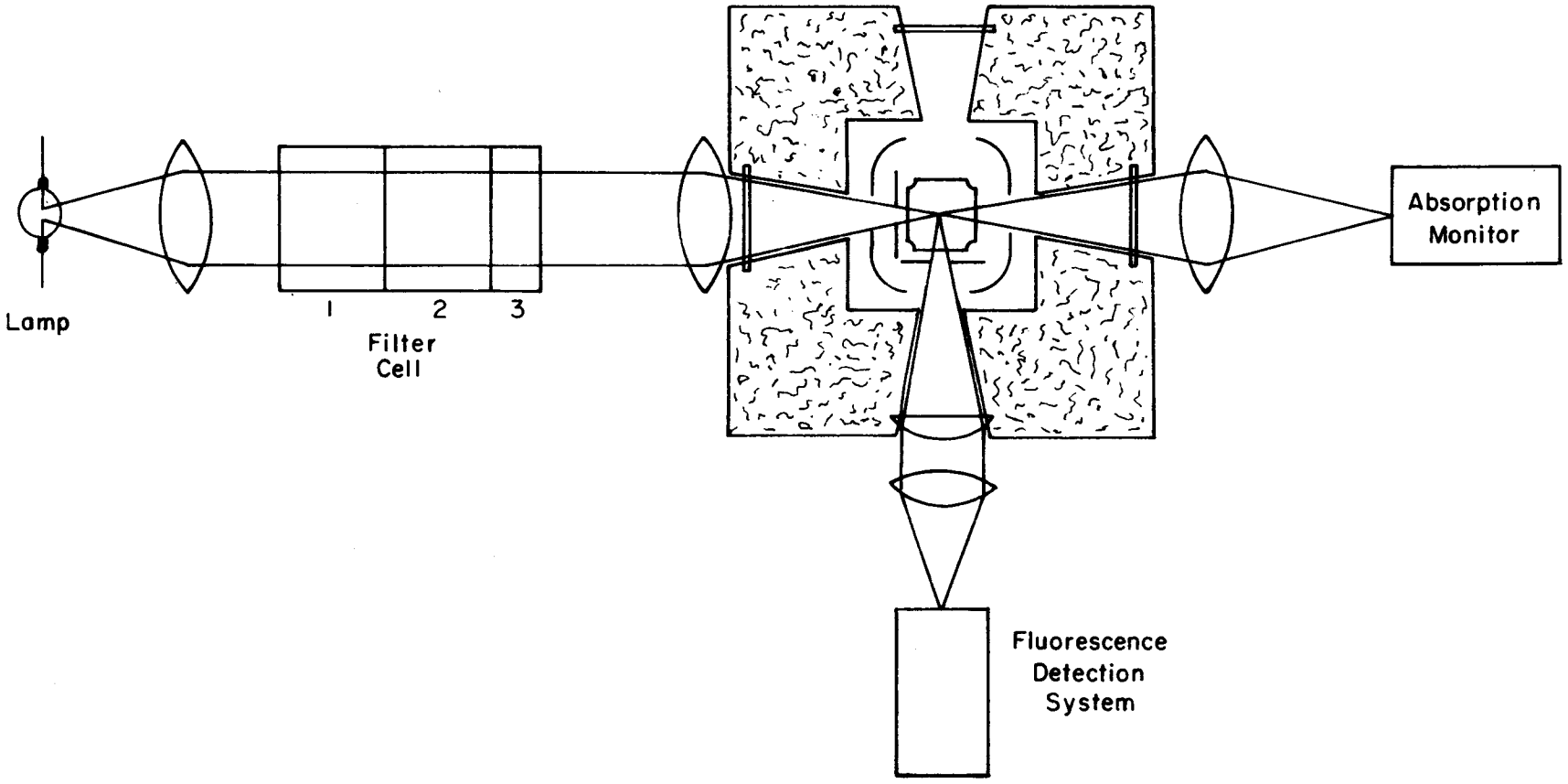

Figure 2.1 Experimental set up.

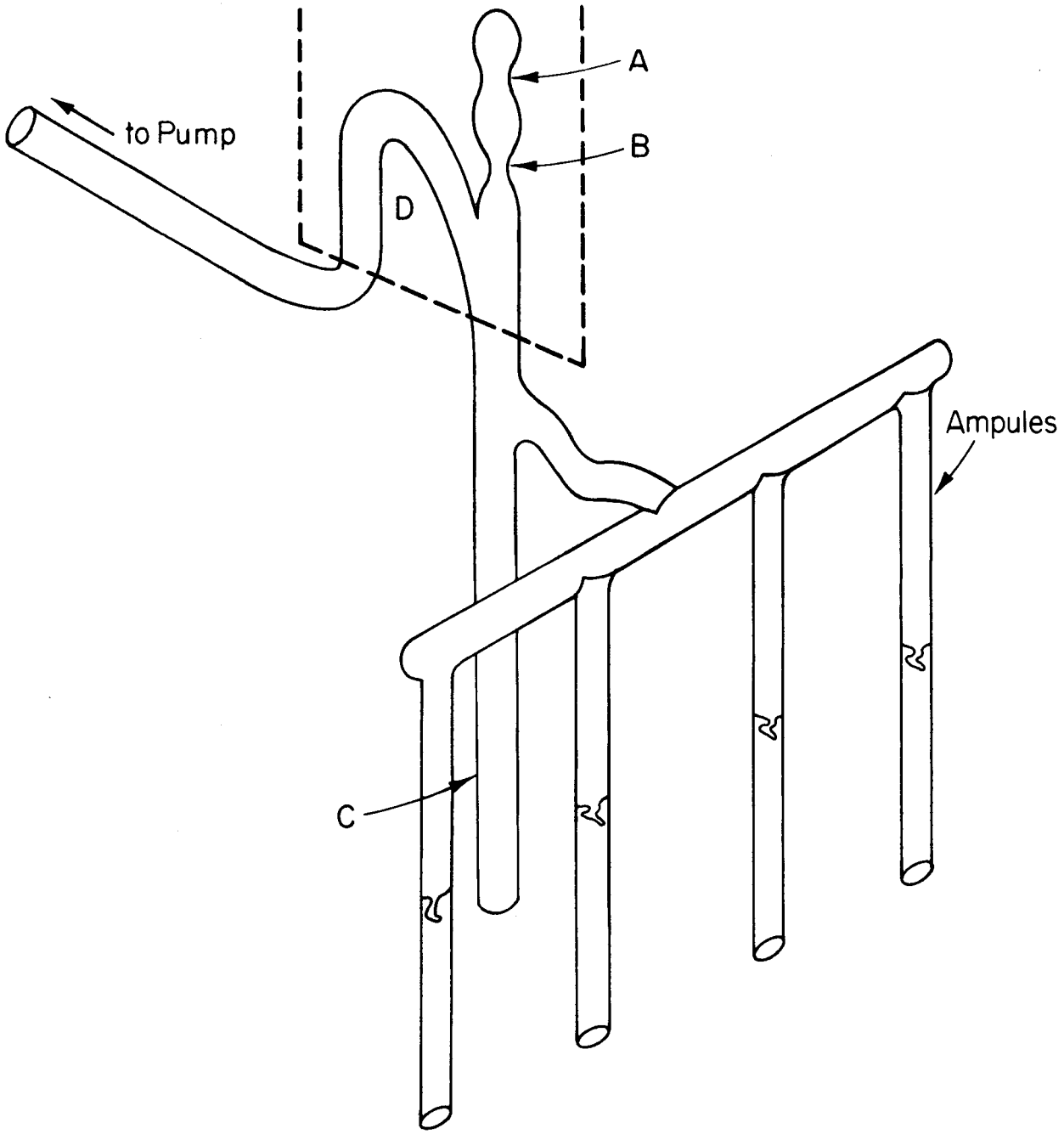

Figure 2.2 Mercury ampule preparation system.

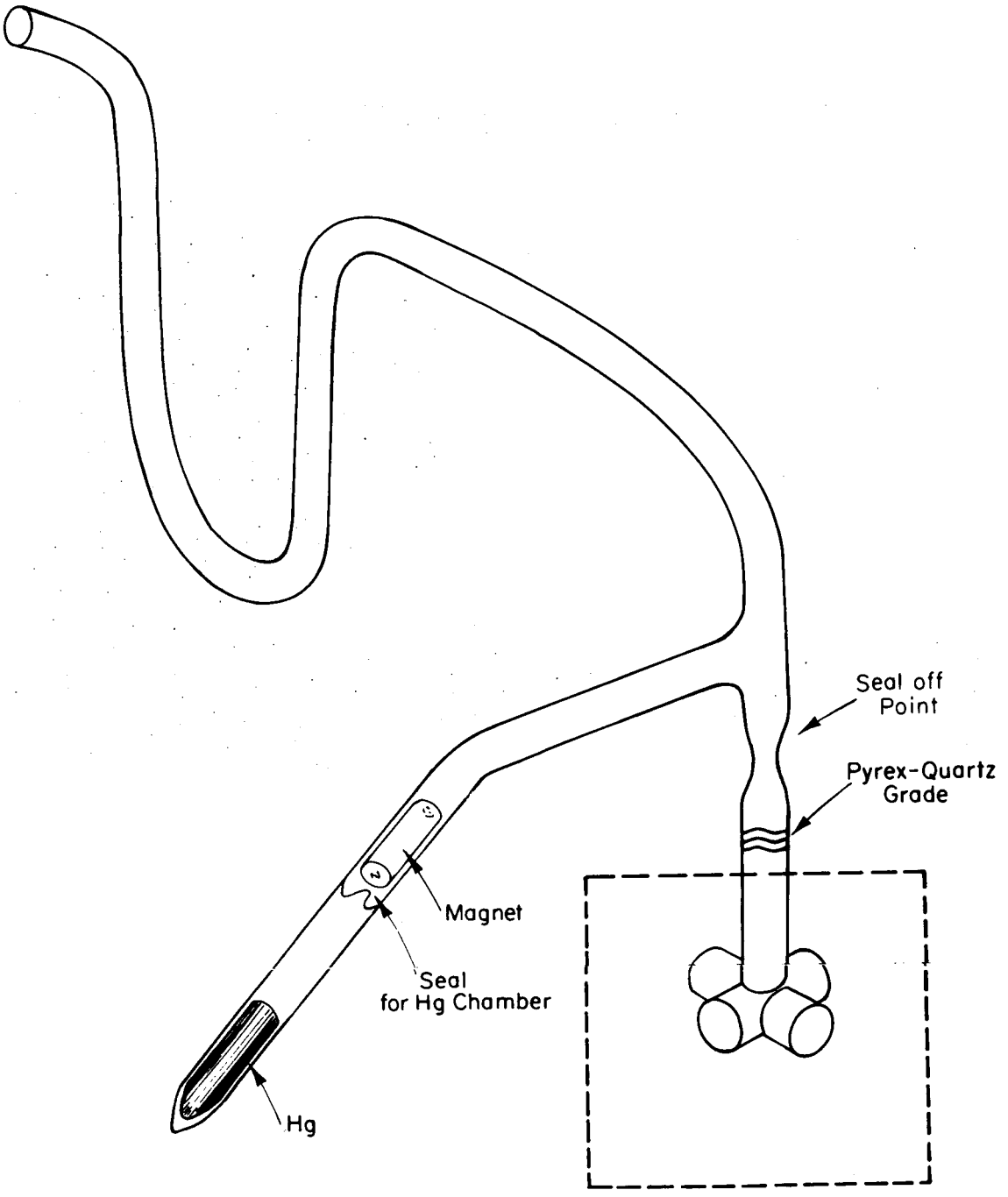

Figure 2.3 Mercury cell distillation system.

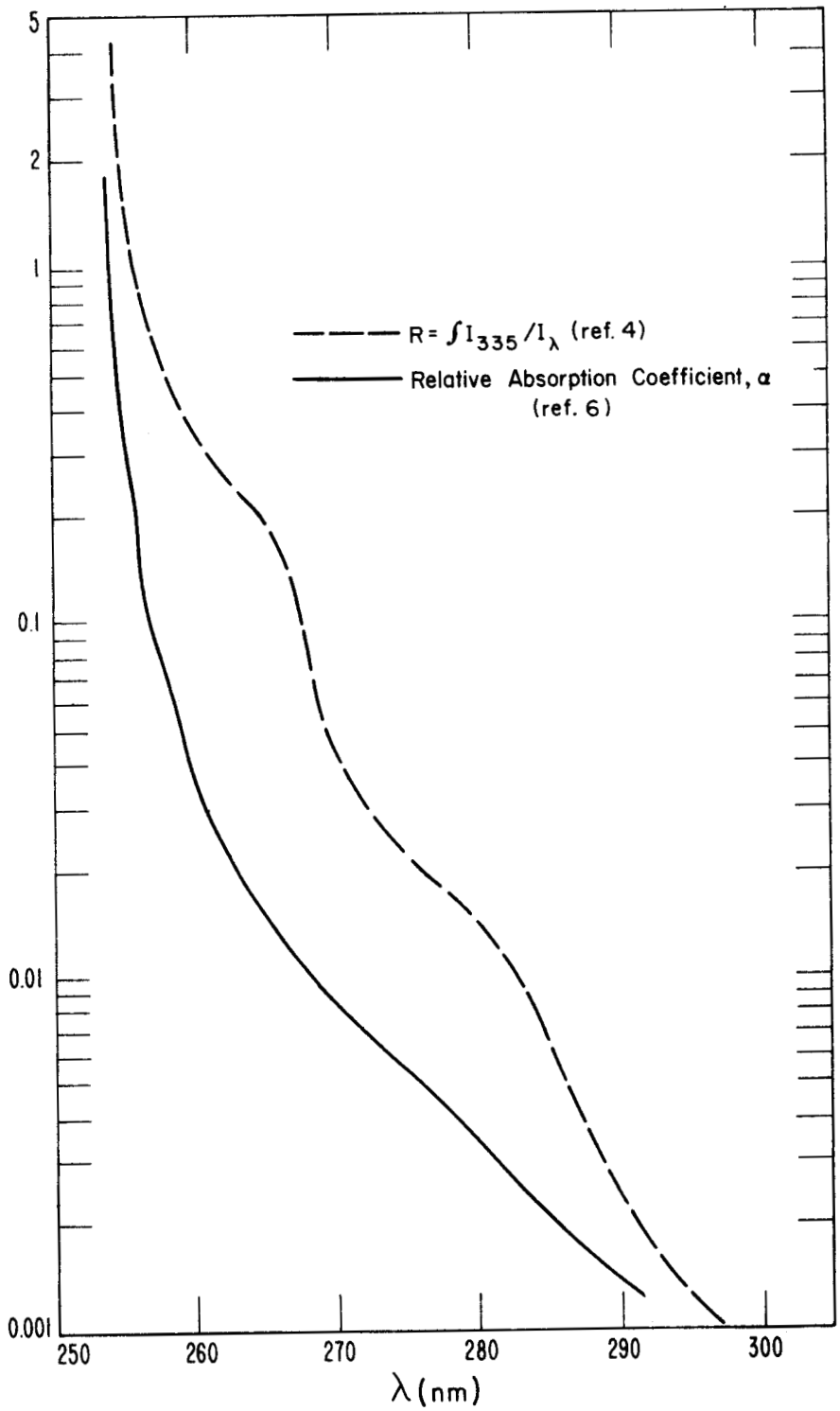

Figure 2.4 Absorption coefficient and integrated band intensity versus wavelength.

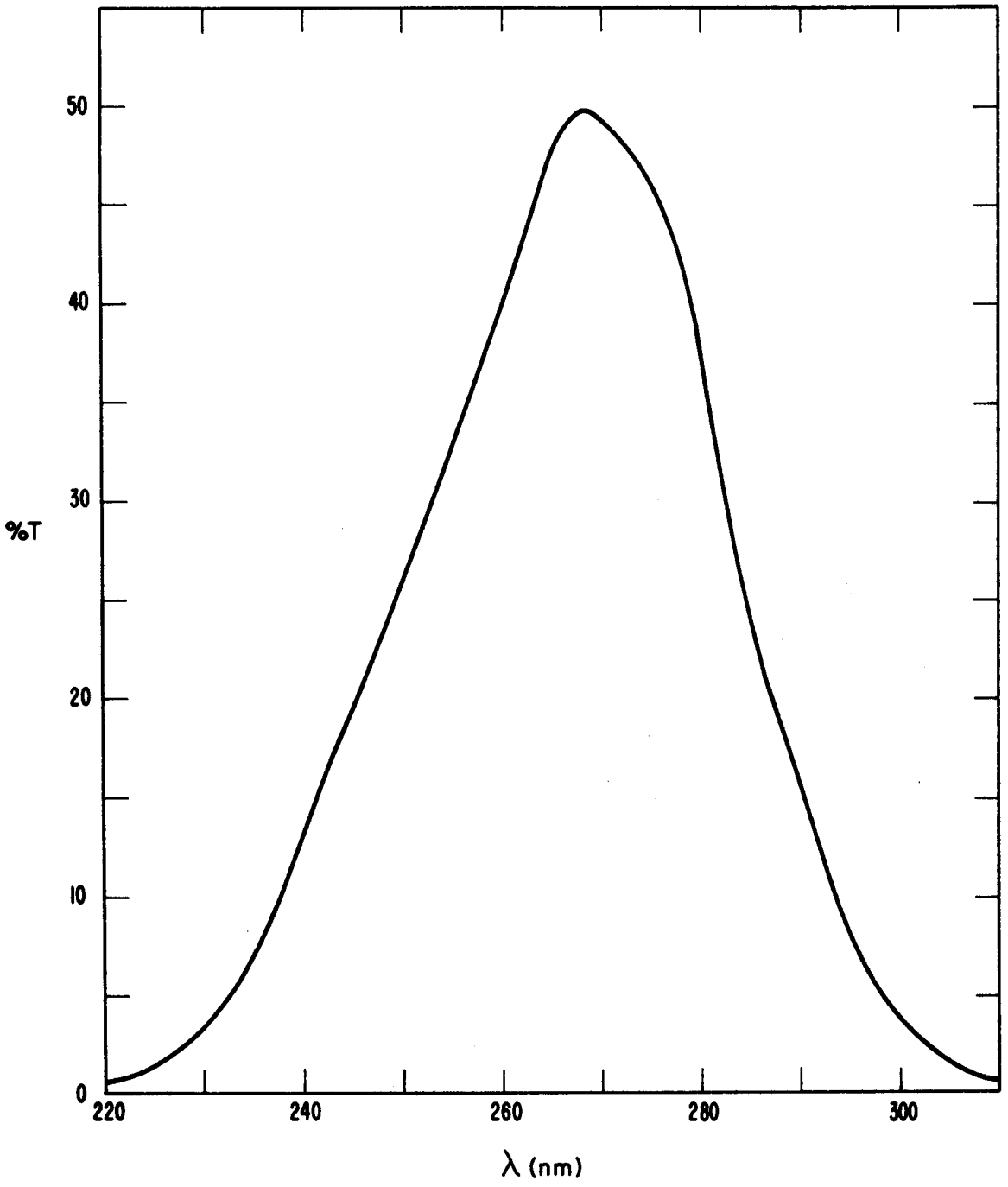

Figure 2.5 Transmission curve of tri-compartment filter.

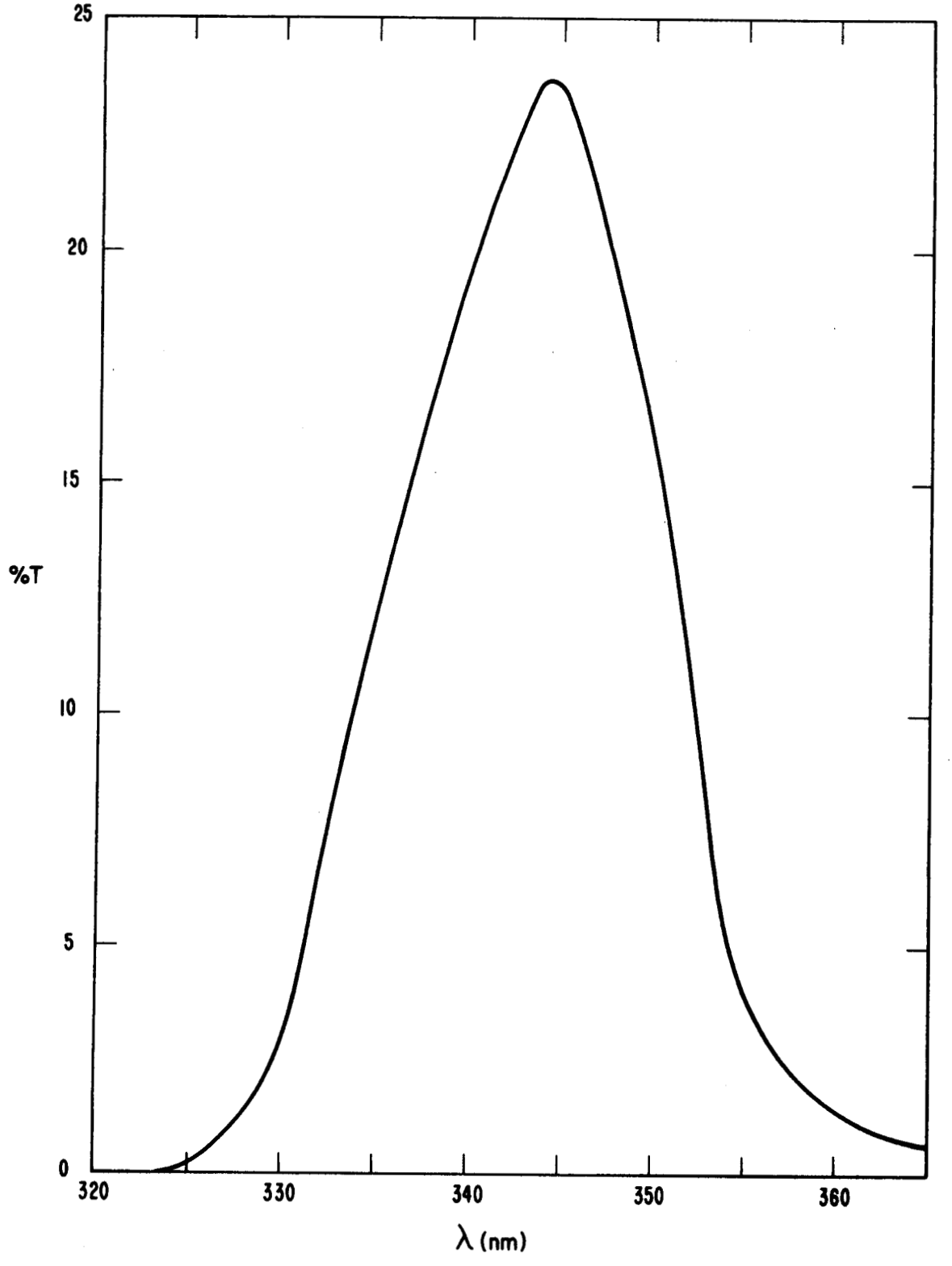

Figure 2.6 Transmission curve of 335 bandpass filter.

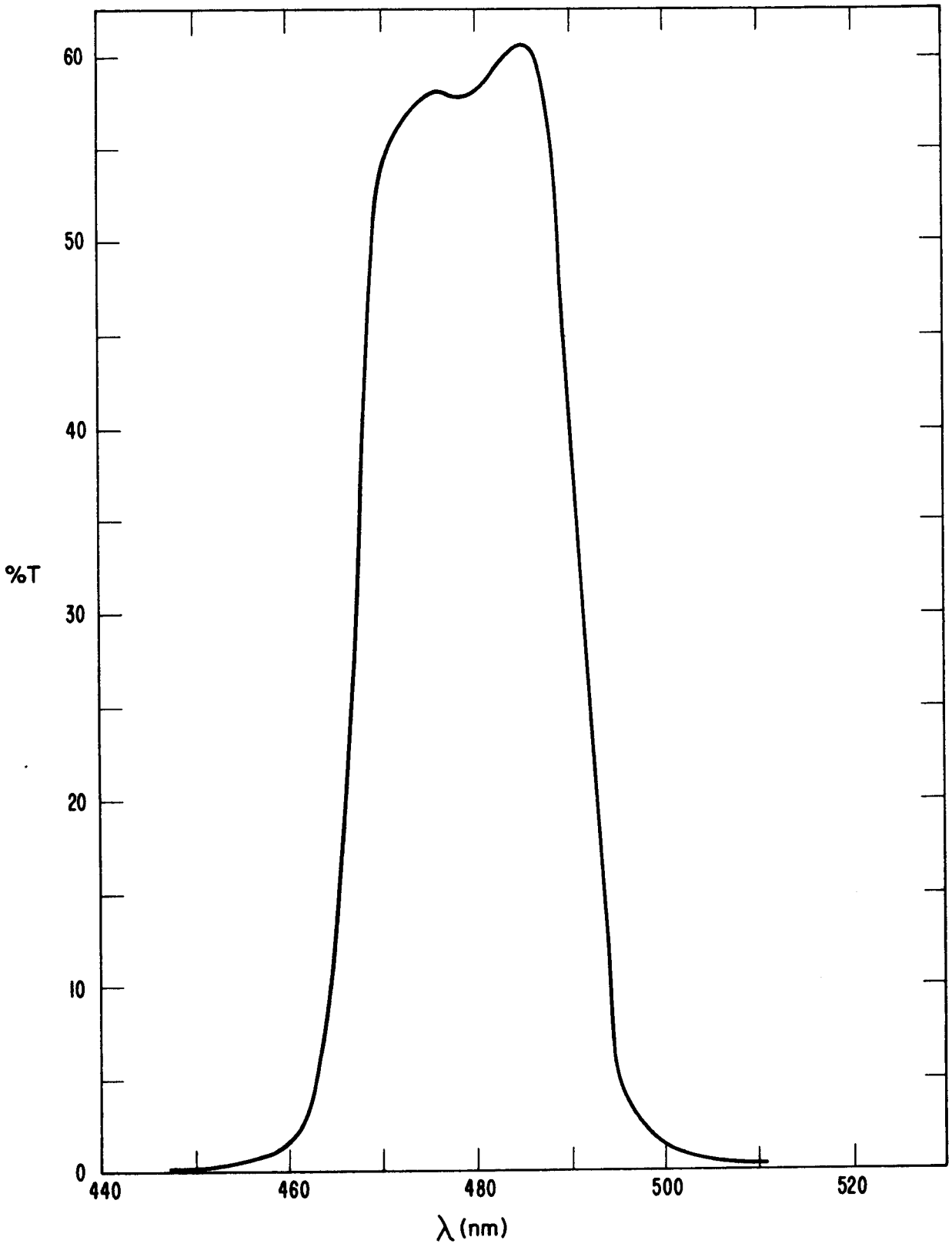

Figure 2.7 Transmission curve of 485 bandpass filter.

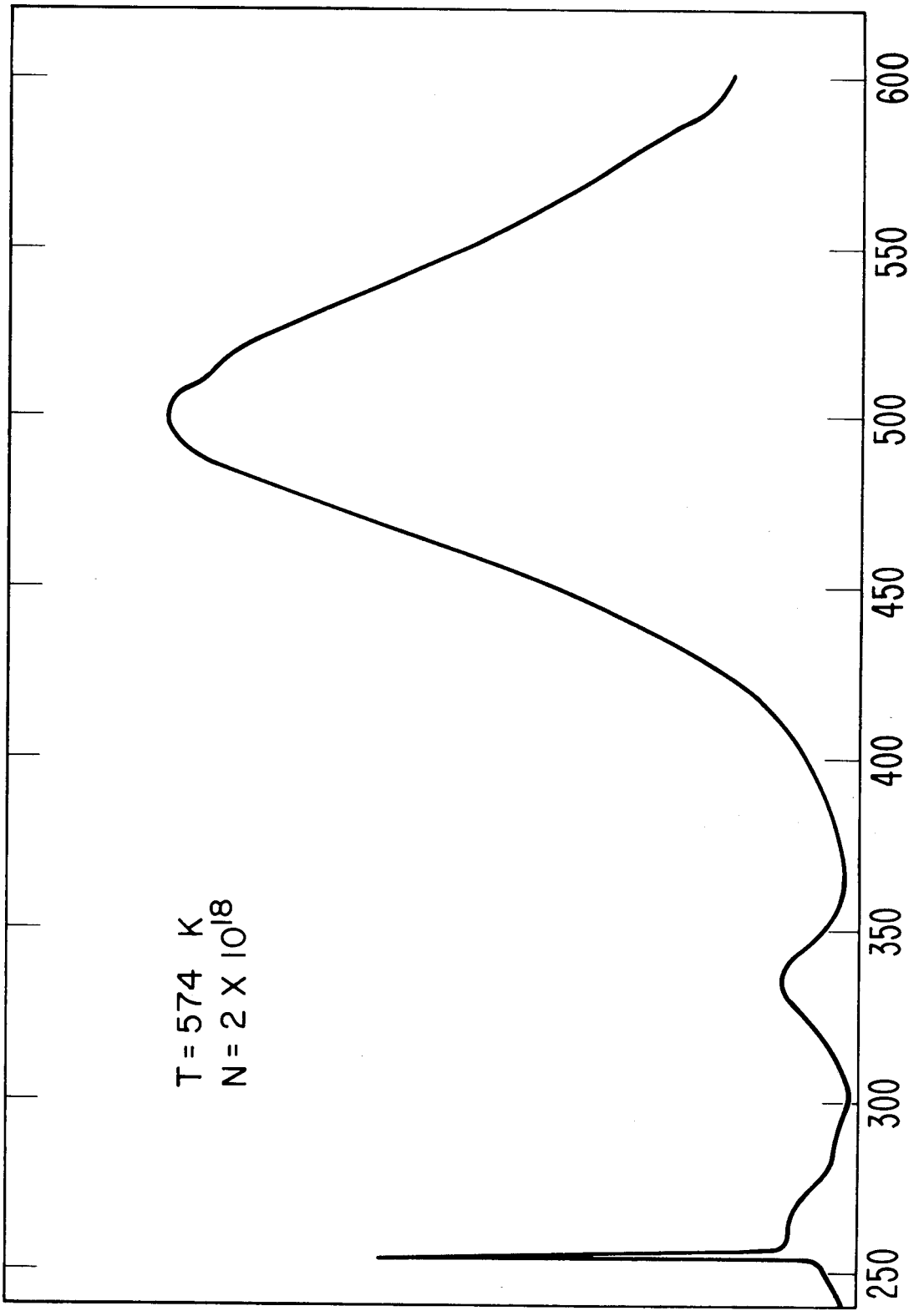

Figure 3.1 Spectral distribution of Hg_2 florescence excited by Xe Arc.

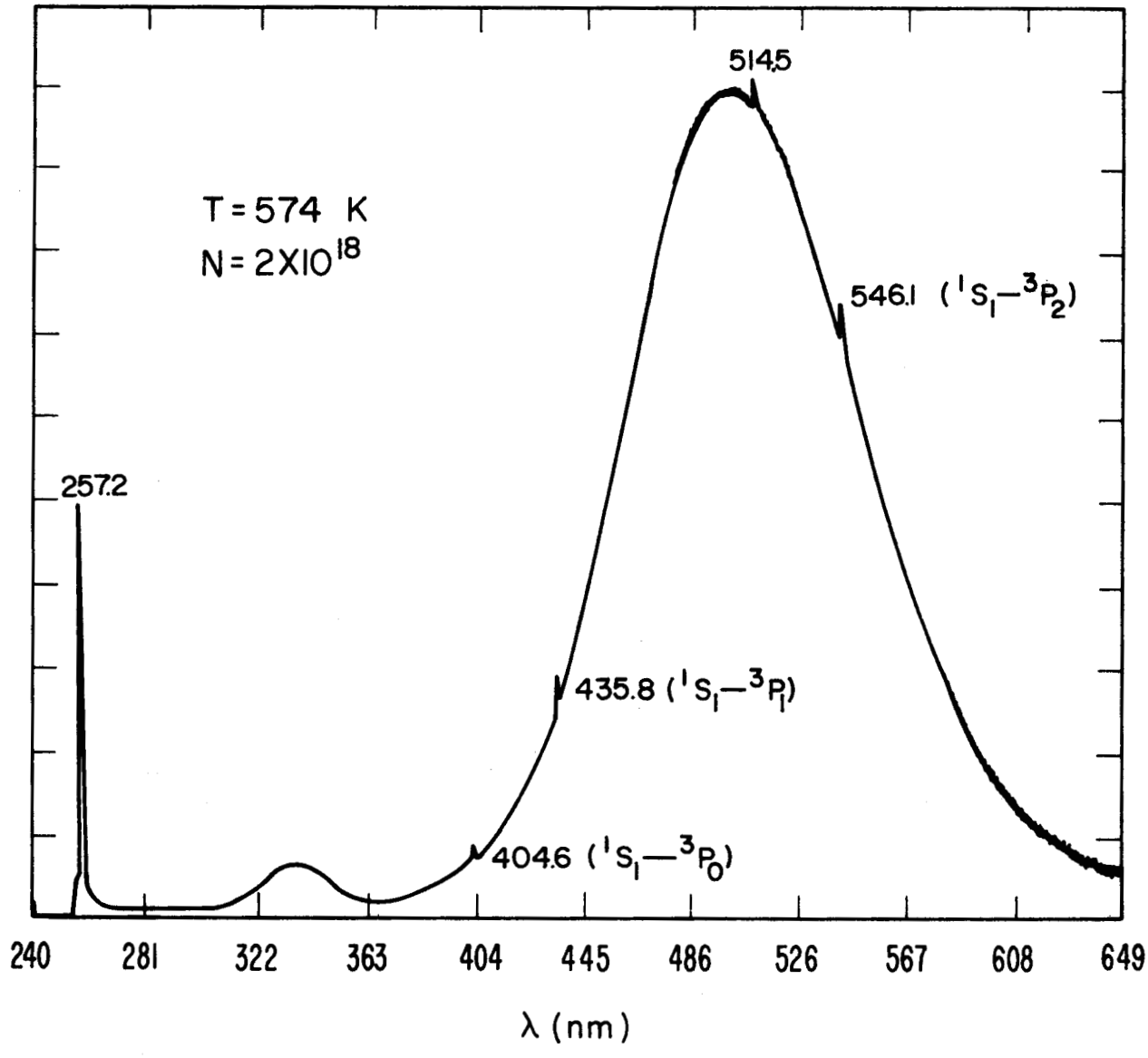

Figure 3.2 Spectral distribution of Hg_2 fluorescence excited by 257.2 nm laser line.

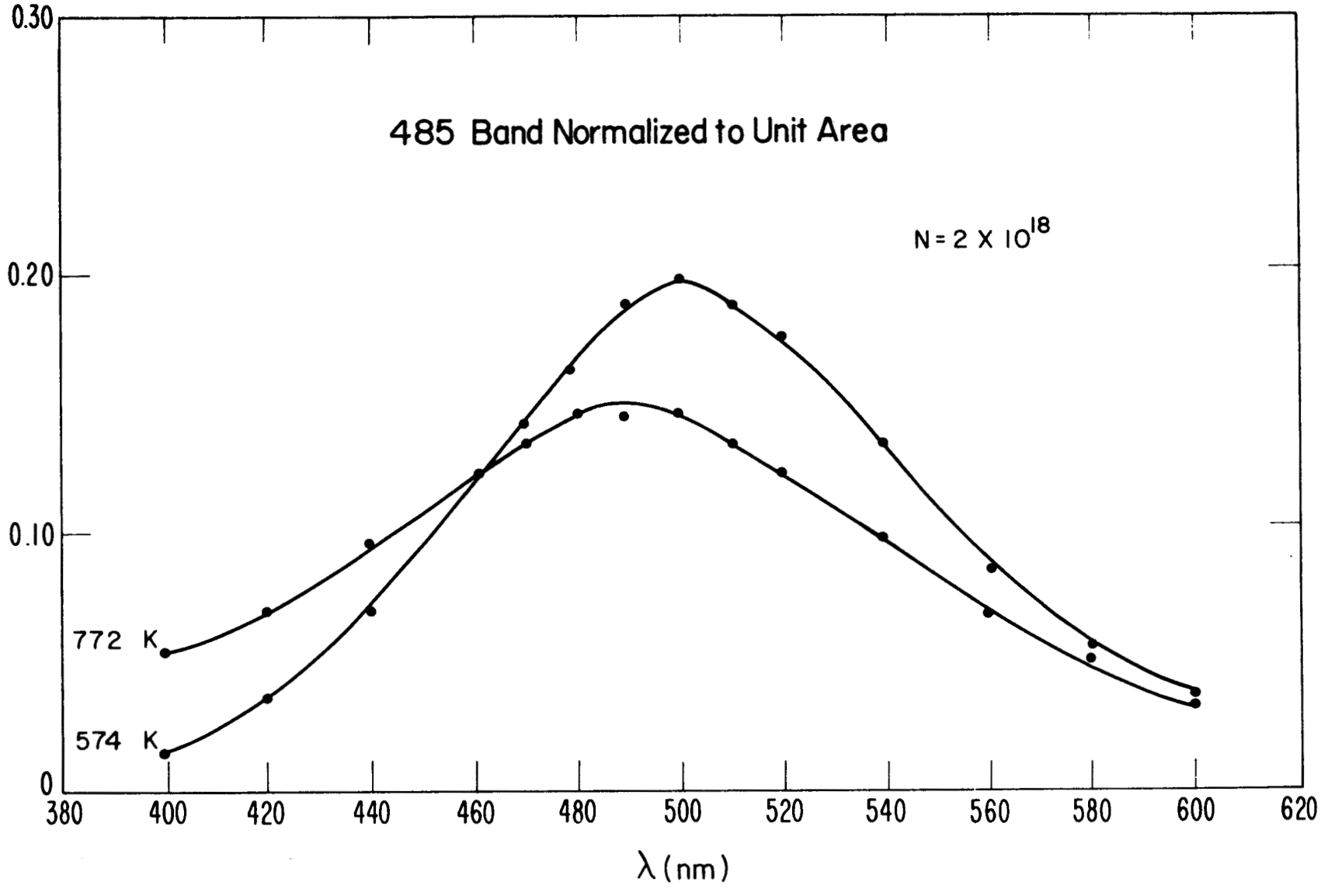

Figure 3.3 Spectral distribution of 485 band at different temperatures.

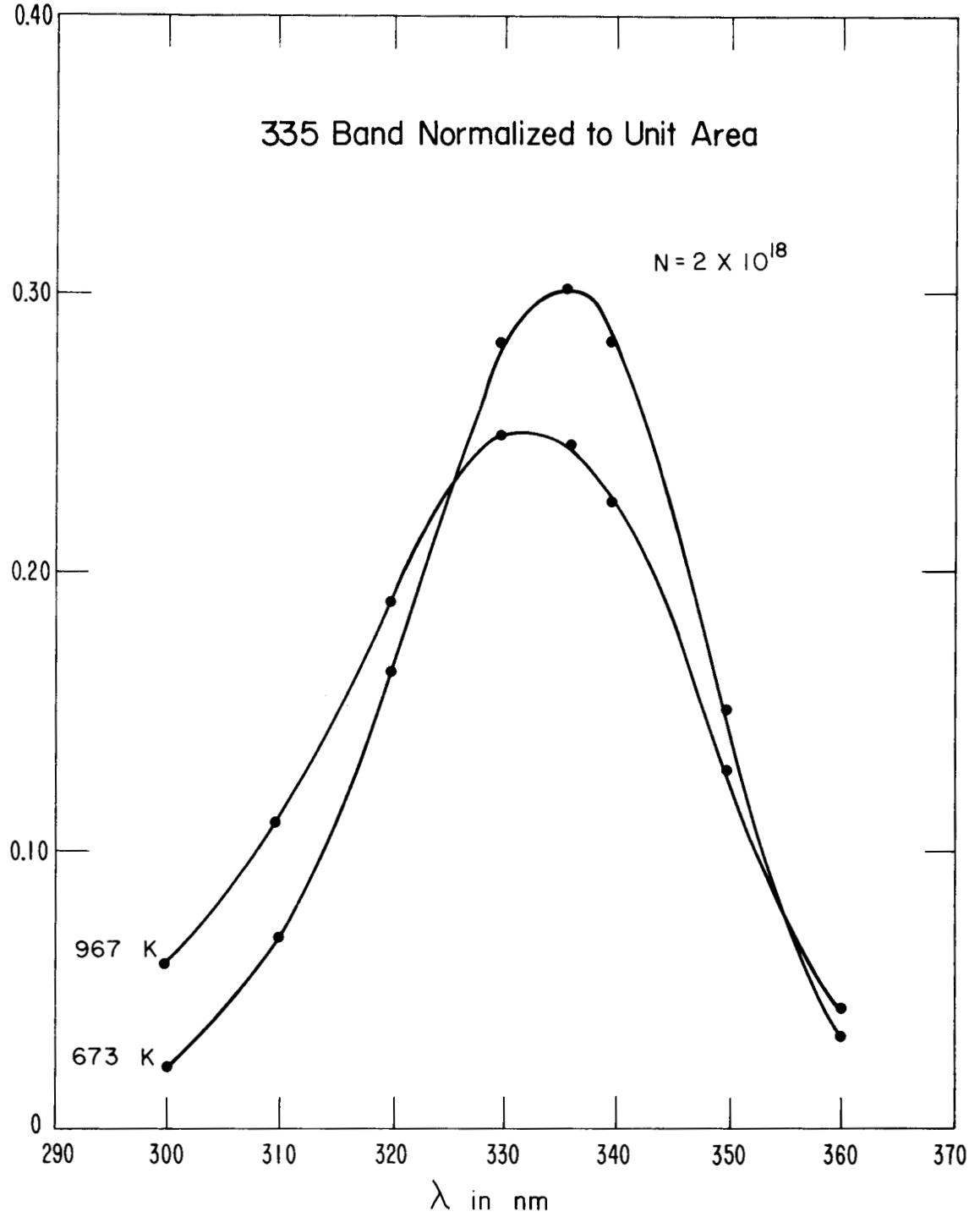

Figure 3.4 Spectral distribution of 335 band at different temperatures.

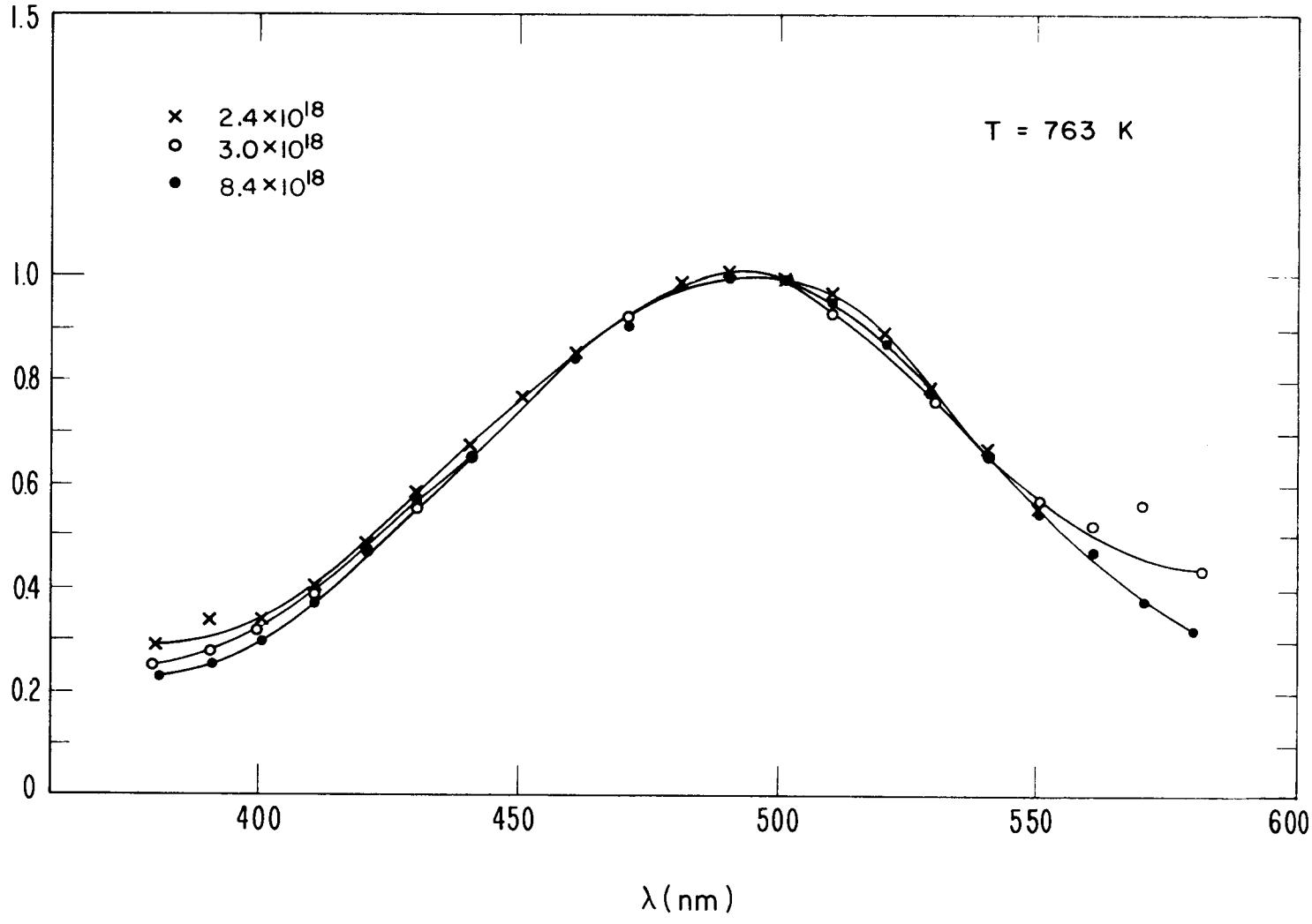

Figure 3.5 Spectral distribution of 485 band at different vapor densities.

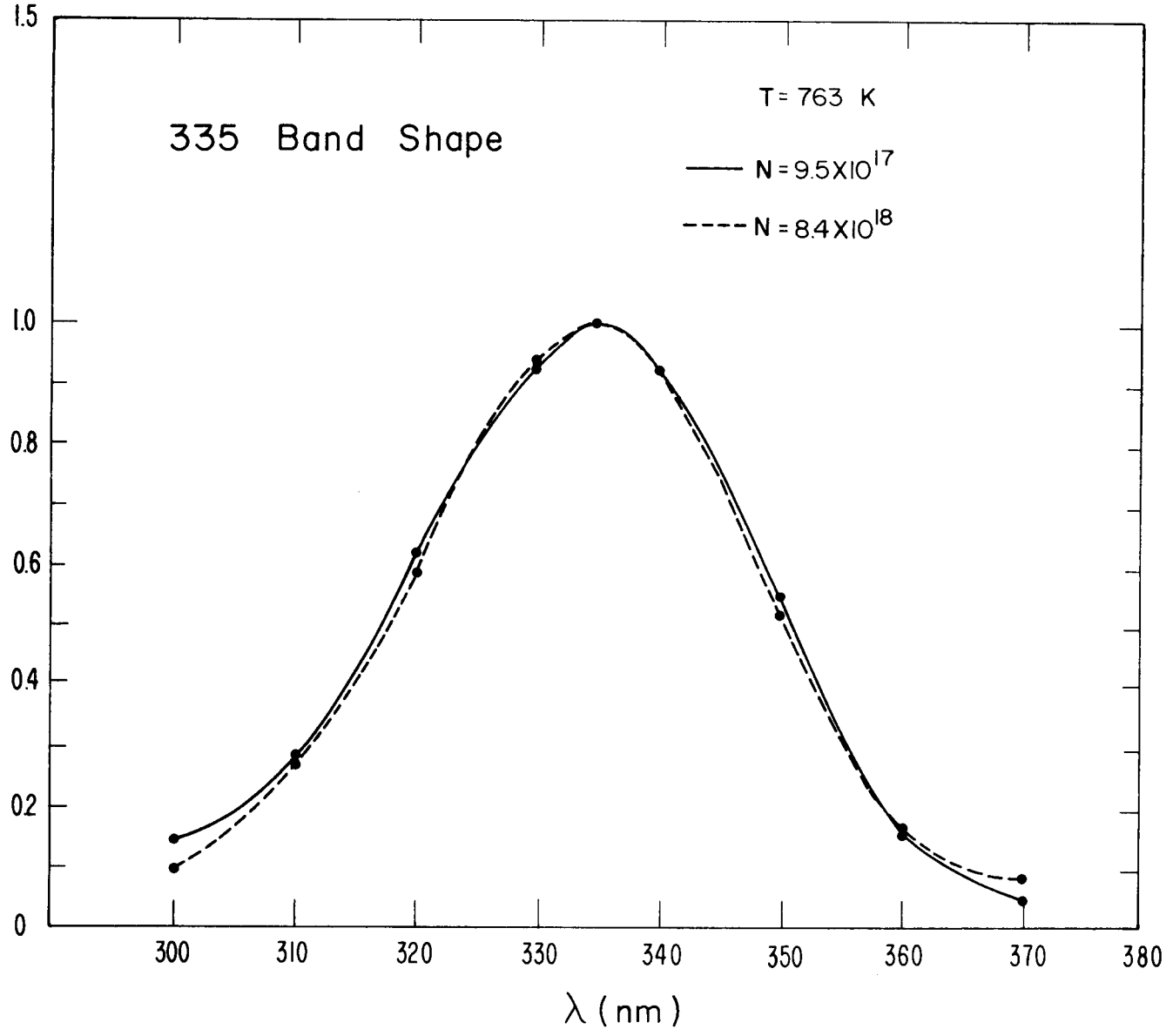

Figure 3.6 Spectral distribution of 335 band at different vapor densities.

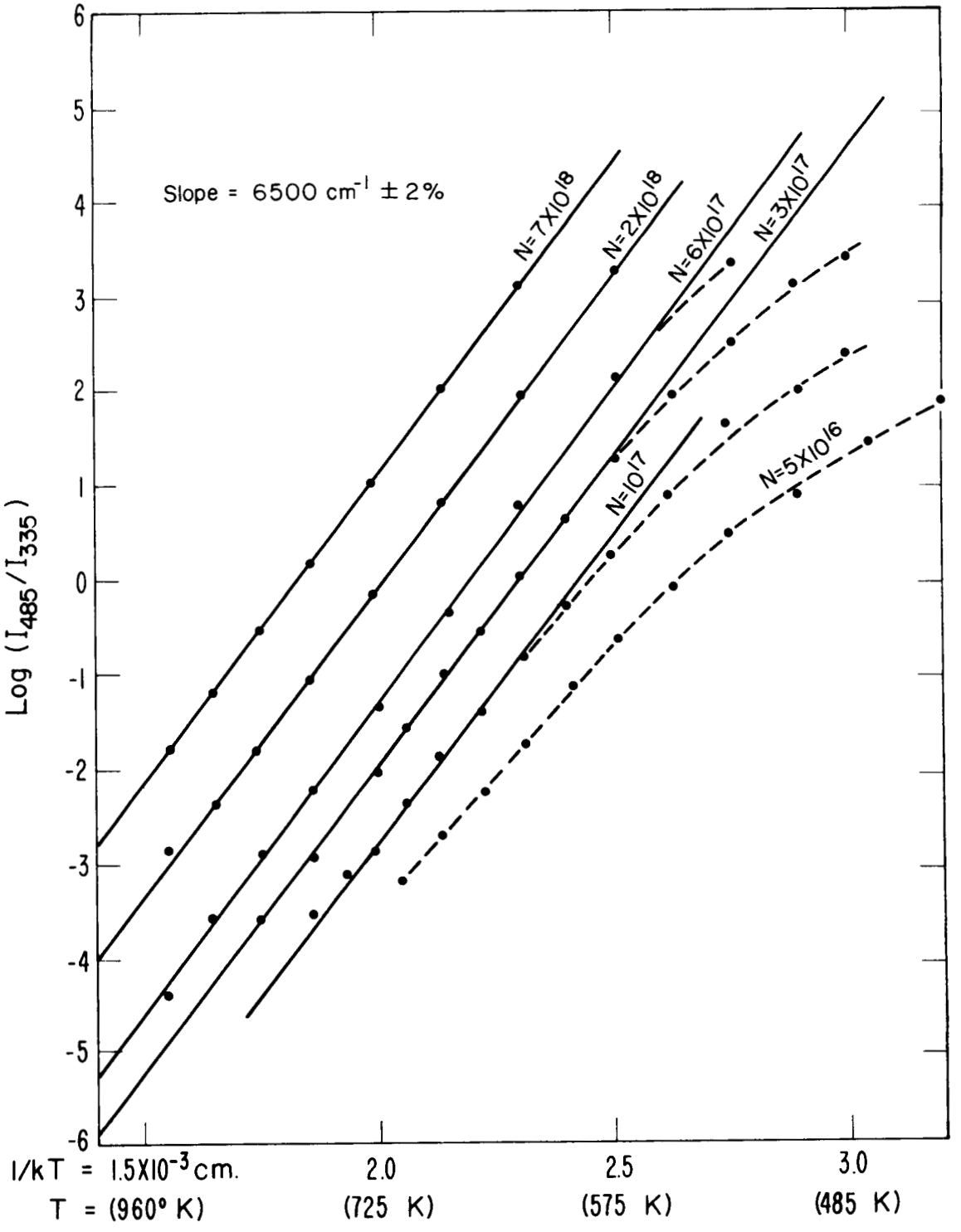

Figure 3.7 Ratio of 485/335 band intensities versus temperature.

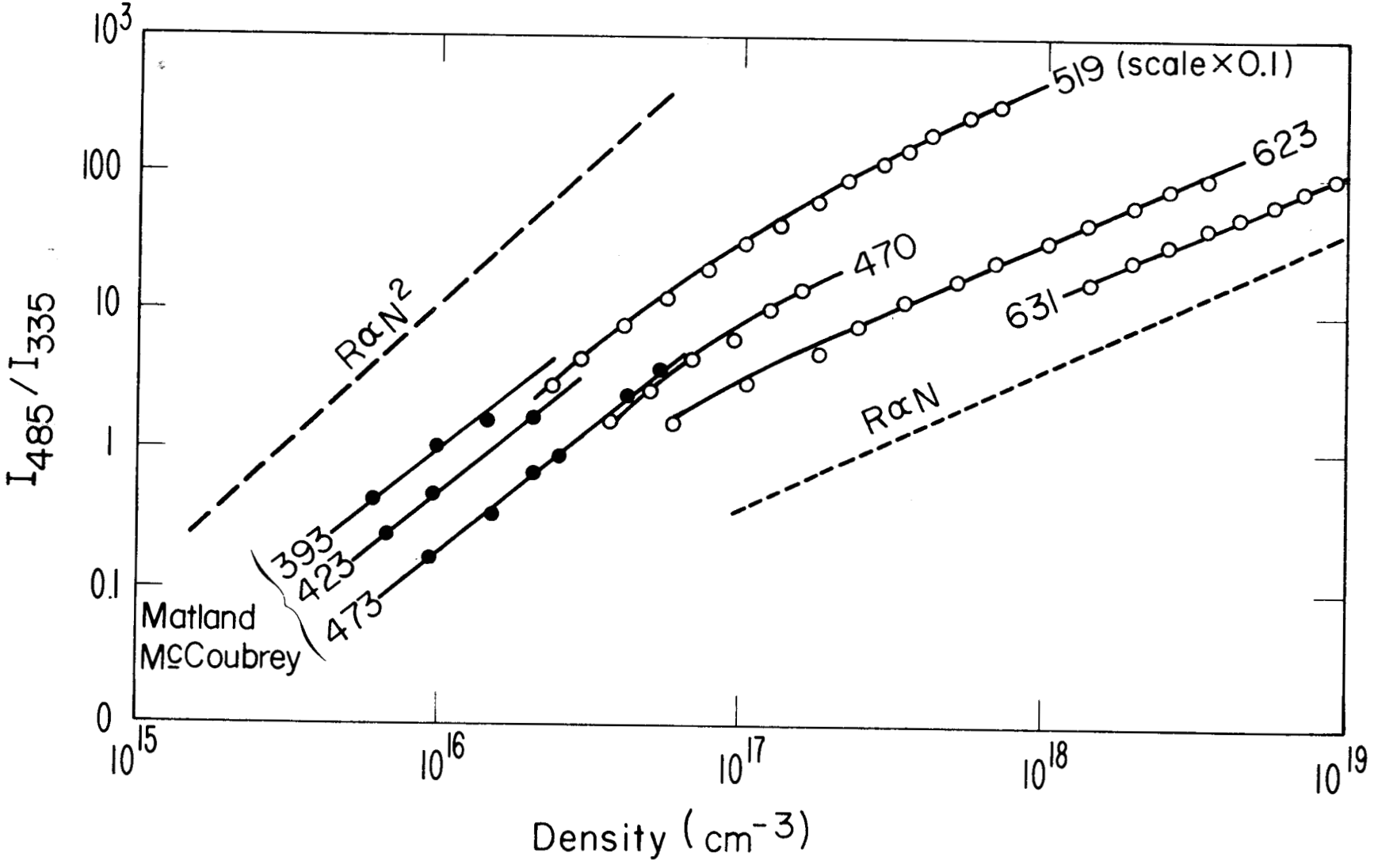

Figure 3.8 Ratio of 485/335 band intensities versus density.

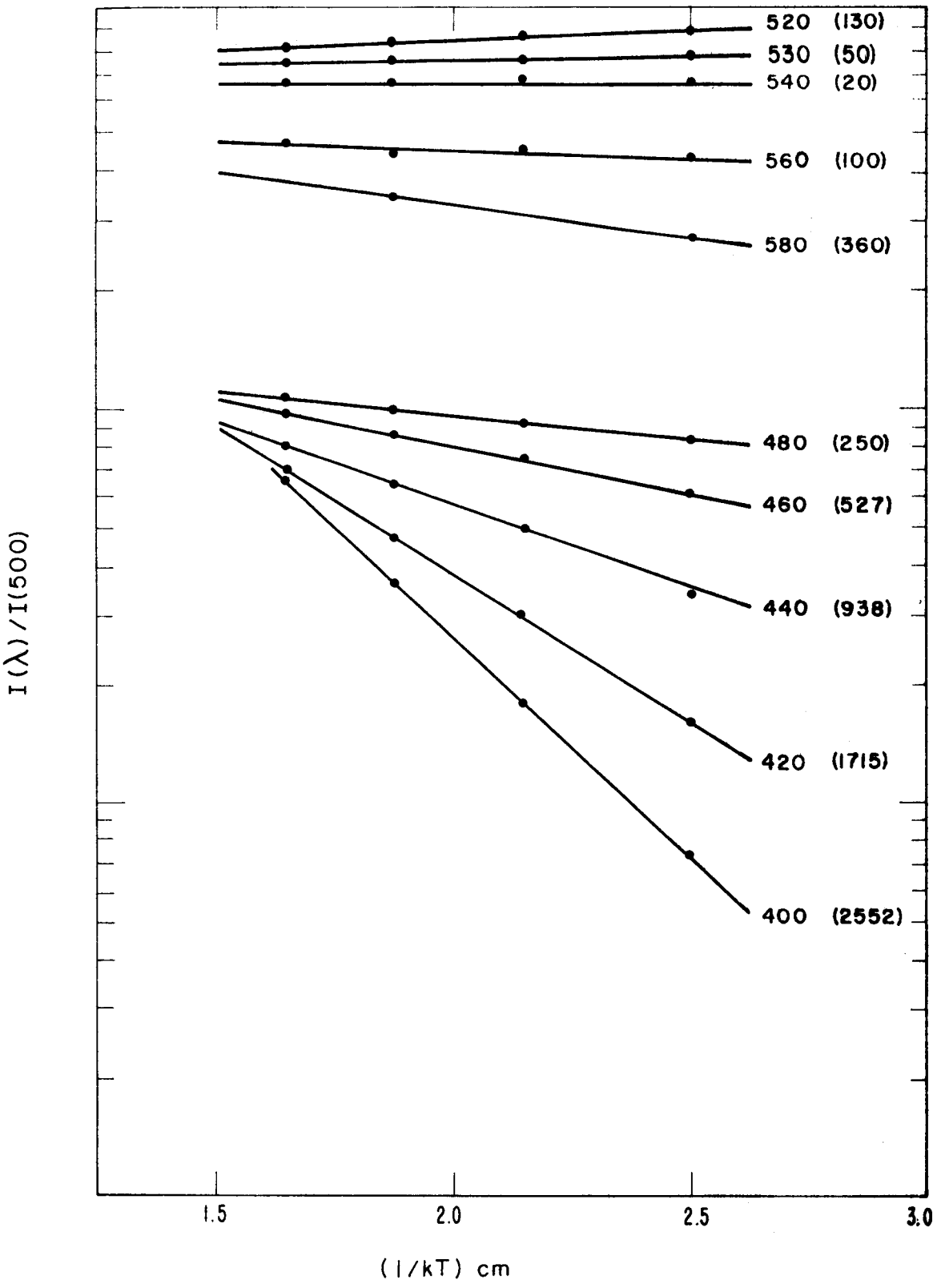

Figure 3.9 Normalized intensities versus temperature in the 485 band.

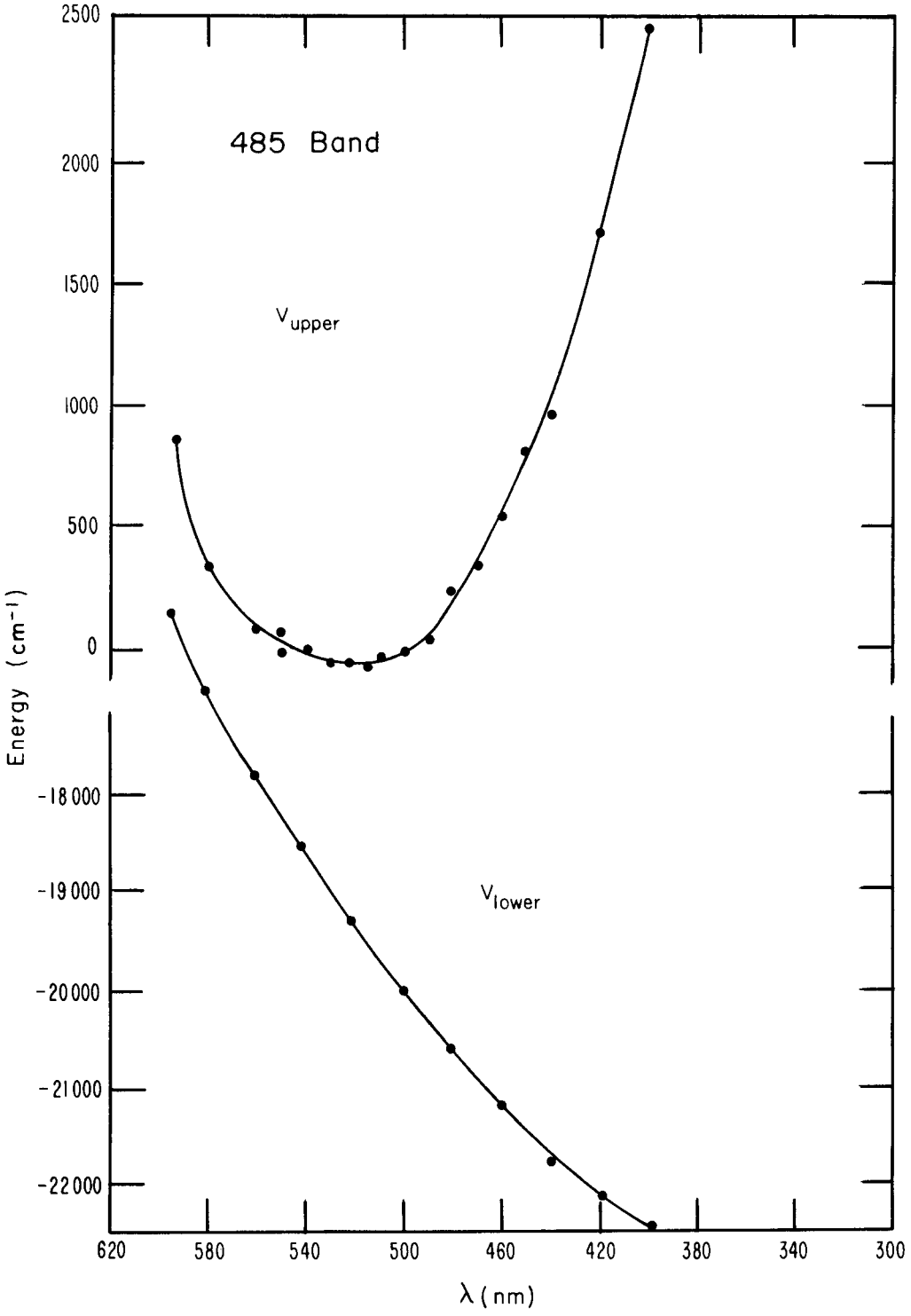

Figure 3.10 Potentials corresponding to the 485 band.

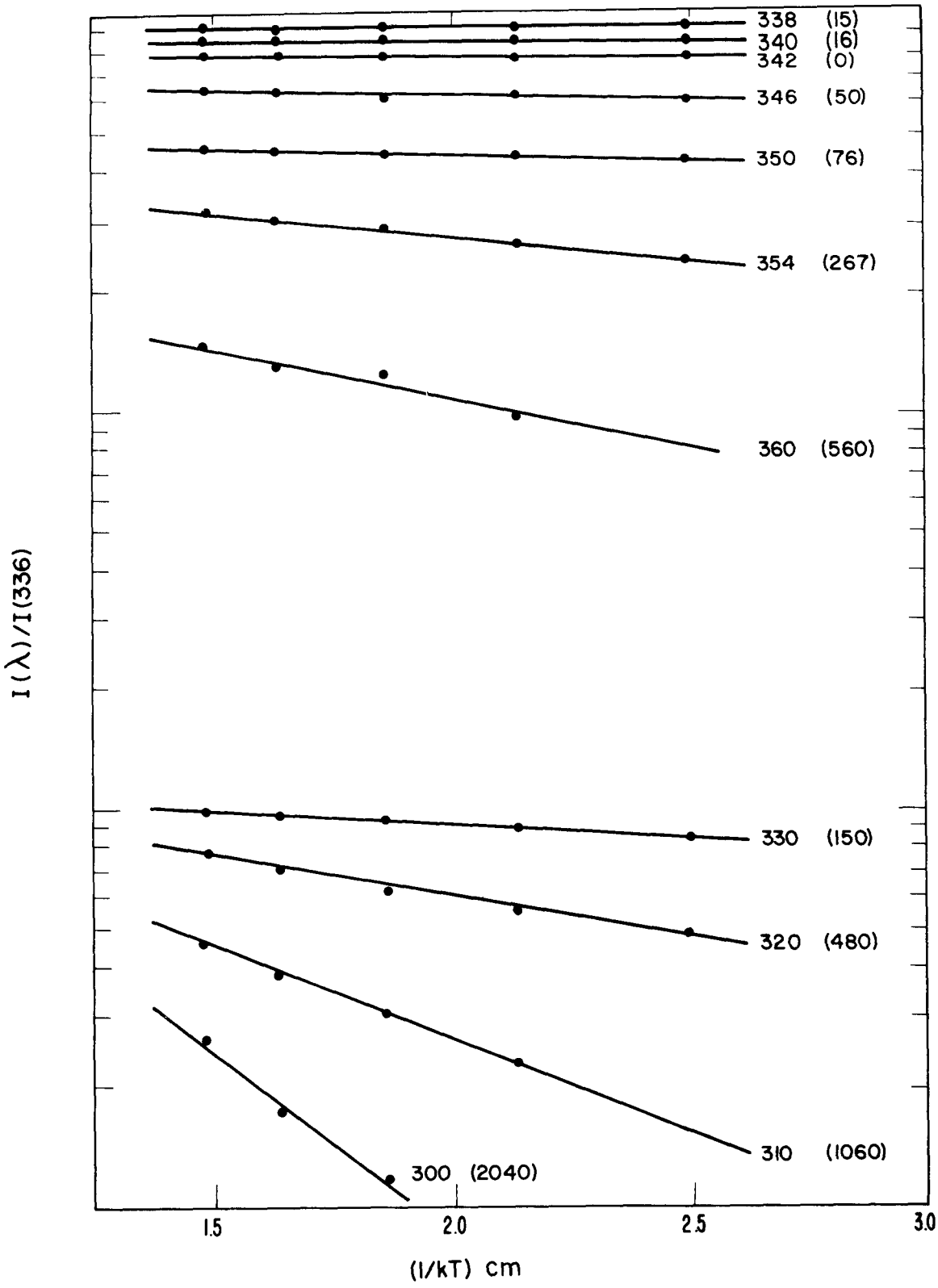

Figure 3.11 Normalized intensities versus temperature in the 335 band.

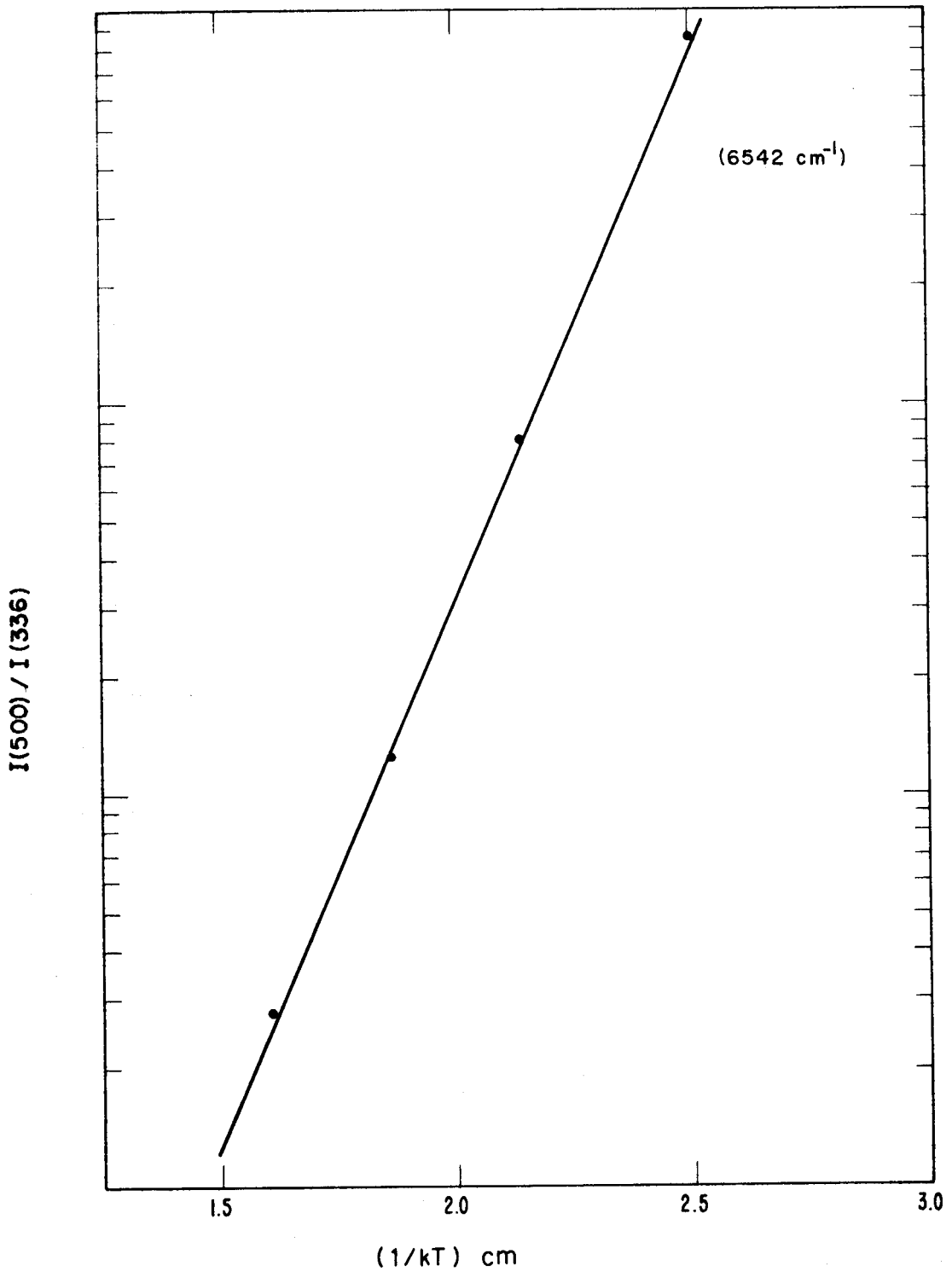

Figure 3.12 Ratio of 485/335 versus temperature.

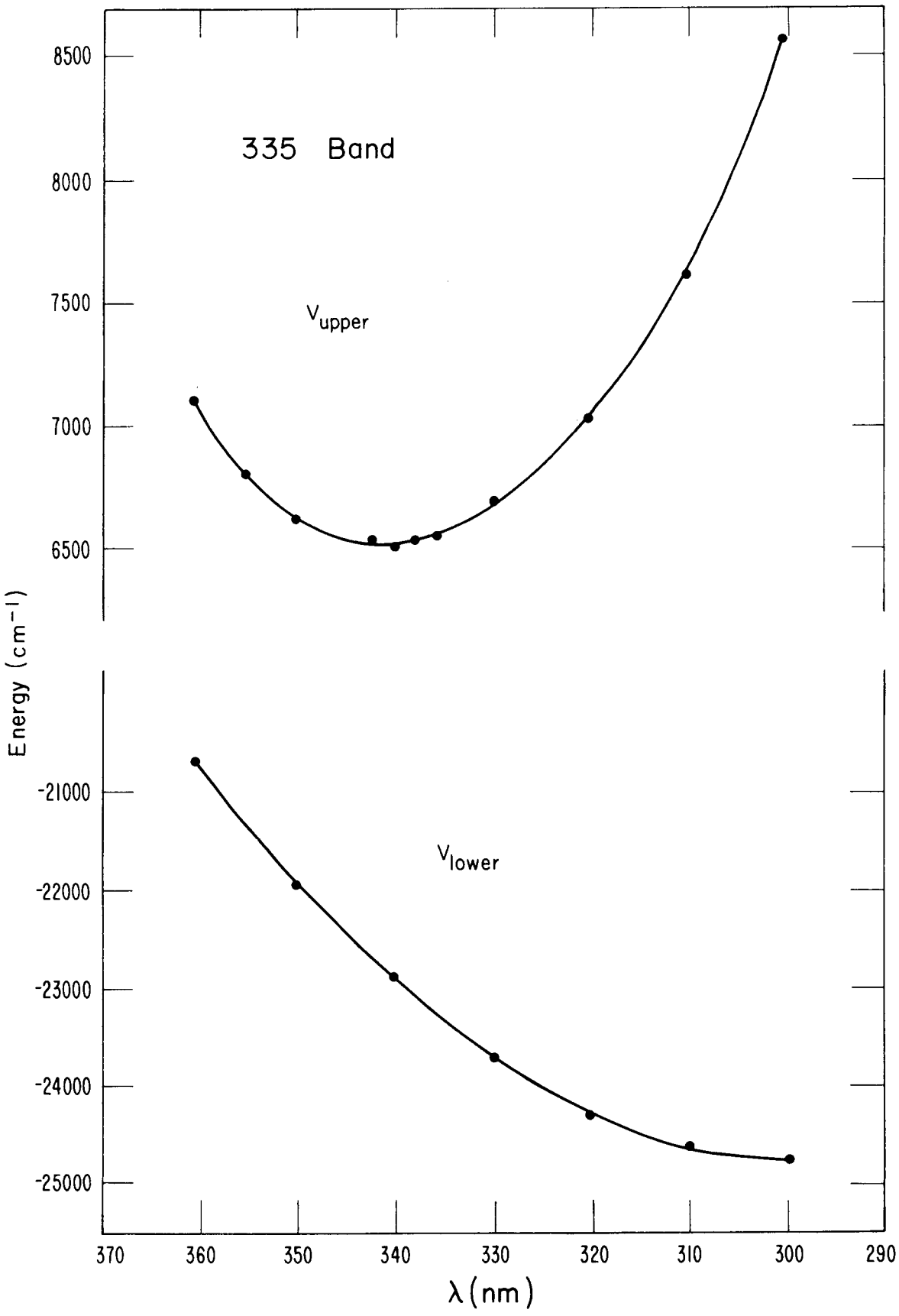

Figure 3.13 Potentials corresponding to the 335 band.

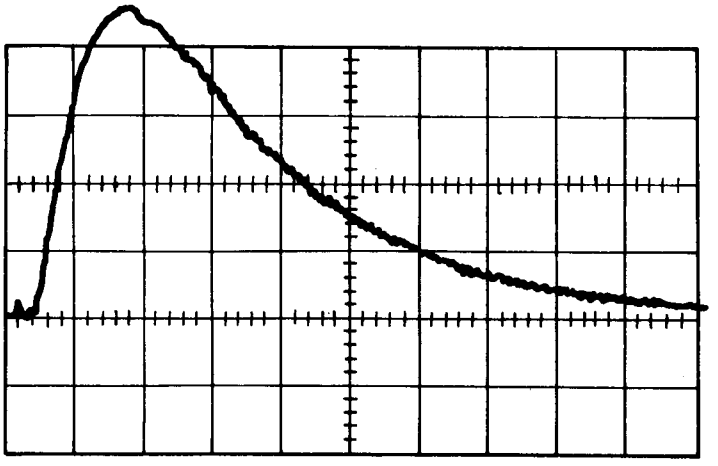

(a) 10 μsec / Div.

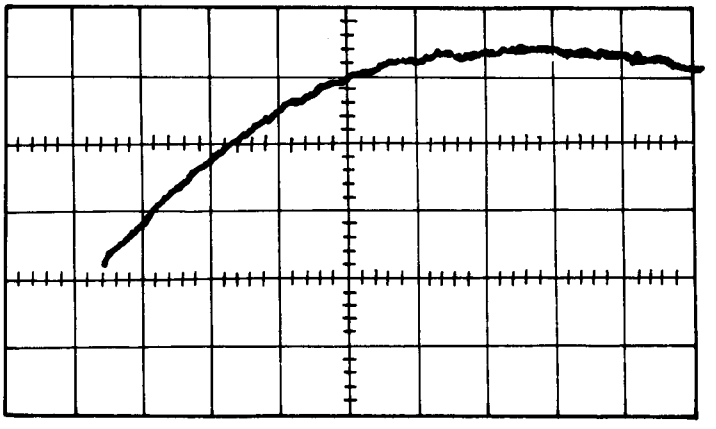

(b) 2 μsec / Div.

Figure 4.1 Time history of the 485 fluorescence band. (a) 10μsec/division and (b) 2 μsec/division.

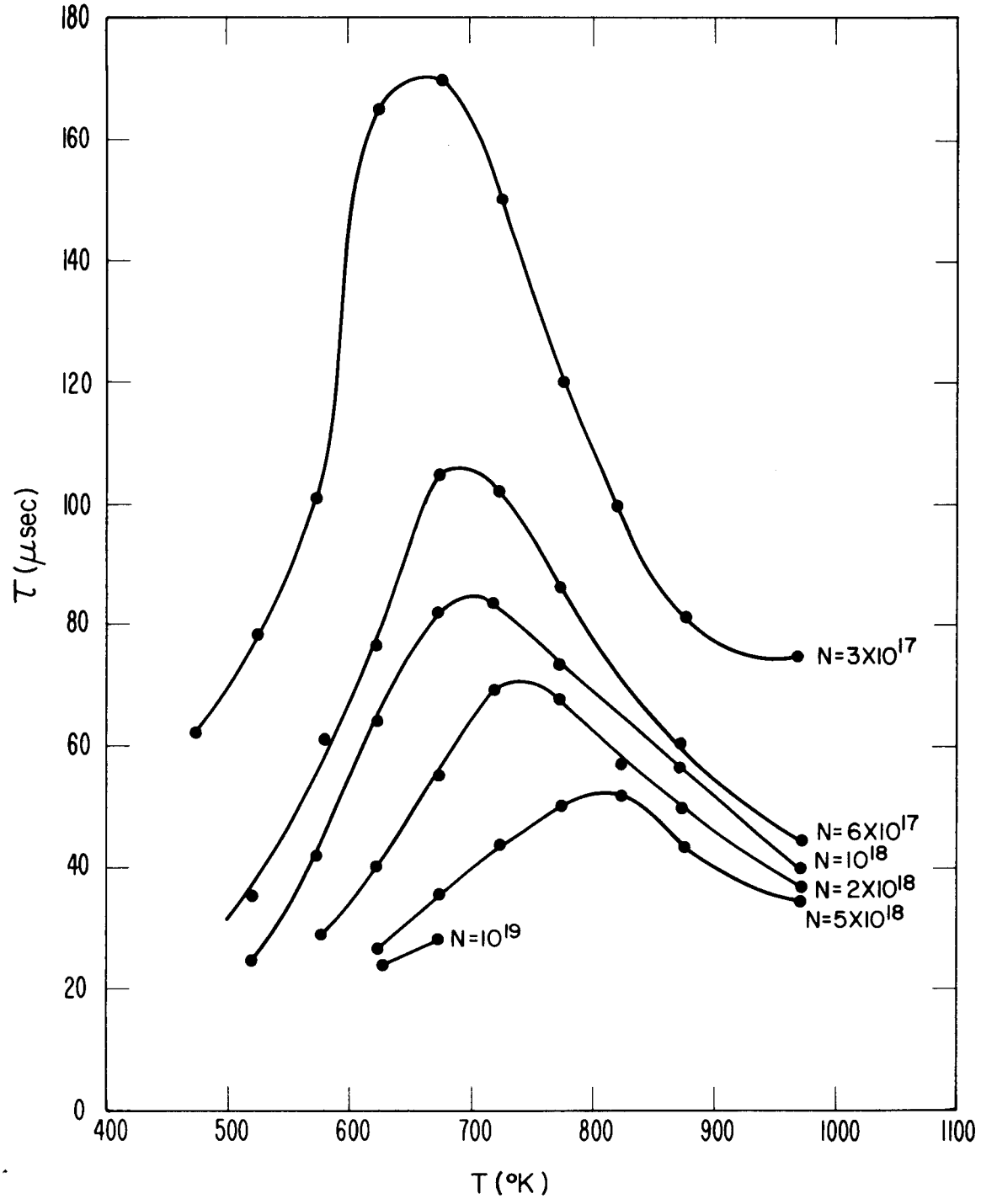

Figure 4.2 Long time decay constant versus temperature and density.

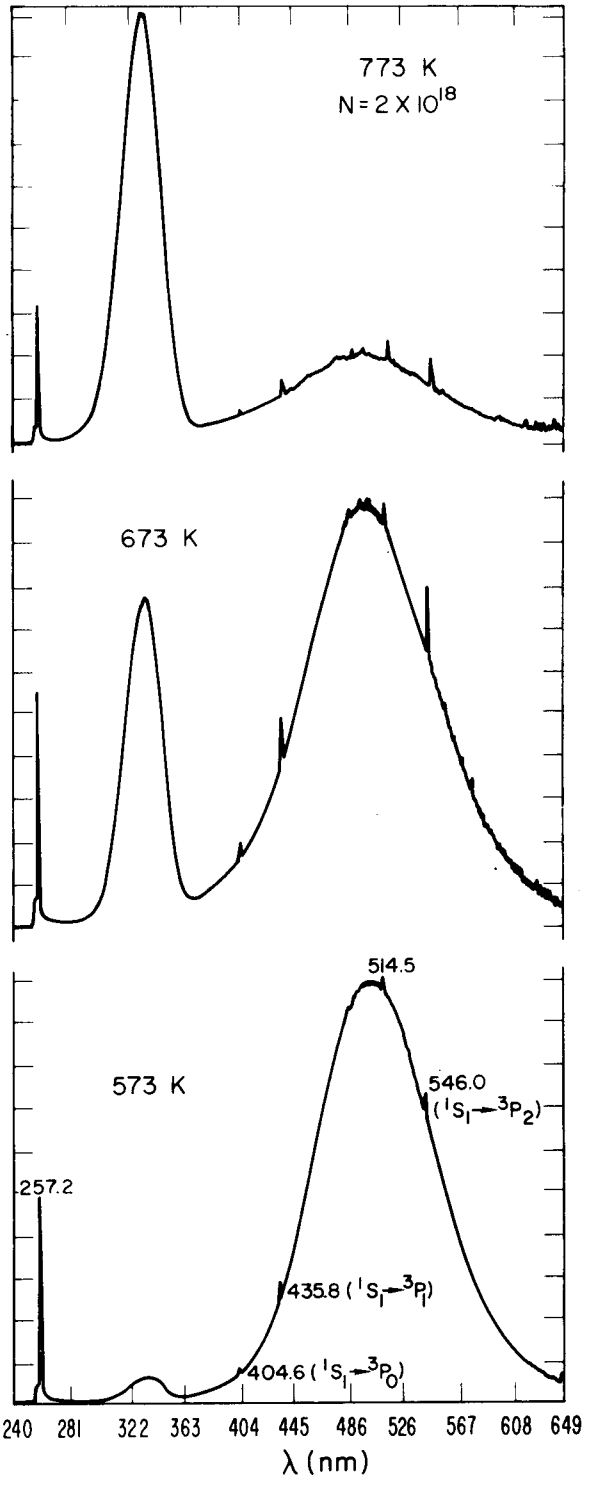

Figure 4.3 Fluorescence spectrum at various temperatures for a fixed atomic density of 2 x 10^{18} cm^{-3}.

NBS TECHNICAL PUBLICATIONS

PERIODICALS

JOURNAL OF RESEARCH reports National Bureau of Standards research and development in physics, mathematics, and chemistry. Comprehensive scientific papers give complete details of the work, including laboratory data, experimental procedures, and theoretical and mathematical analyses. Illustrated with photographs, drawings, and charts. Includes listings of other NBS papers as issued.

Published in two sections, available separately:

- **Physics and Chemistry (Section A)**

Papers of interest primarily to scientists working in these fields. This section covers a broad range of physical and chemical research, with major emphasis on standards of physical measurement, fundamental constants, and properties of matter. Issued six times a year. Annual subscription: Domestic, $17.00; Foreign, $21.25.

- **Mathematical Sciences (Section B)**

Studies and compilations designed mainly for the mathematician and theoretical physicist. Topics in mathematical statistics, theory of experiment design, numerical analysis, theoretical physics and chemistry, logical design and programming of computers and computer systems. Short numerical tables. Issued quarterly. Annual subscription: Domestic, $9.00; Foreign, $11.25.

DIMENSIONS/NBS (formerly Technical News Bulletin)—This monthly magazine is published to inform scientists, engineers, businessmen, industry, teachers, students, and consumers of the latest advances in science and technology, with primary emphasis on the work at NBS.

DIMENSIONS/NBS highlights and reviews such issues as energy research, fire protection, building technology, metric conversion, pollution abatement, health and safety, and consumer product performance. In addition, **DIMENSIONS/NBS** reports the results of Bureau programs in measurement standards and techniques, properties of matter and materials, engineering standards and services, instrumentation, and automatic data processing.

NONPERIODICALS

Monographs—Major contributions to the technical literature on various subjects related to the Bureau's scientific and technical activities.

Handbooks—Recommended codes of engineering and industrial practice (including safety codes) developed in cooperation with interested industries, professional organizations, and regulatory bodies.

Special Publications—Include proceedings of high-level national and international conferences sponsored by NBS, precision measurement and calibration volumes, NBS annual reports, and other special publications appropriate to this grouping such as wall charts and bibliographies.

Applied Mathematics Series—Mathematical tables, manuals, and studies of special interest to physicists, engineers, chemists, biologists, mathematicians, computer programmers, and others engaged in scientific and technical work.

National Standard Reference Data Series—Provides quantitative data on the physical and chemical properties of materials, compiled from the world's literature and critically evaluated. Developed under a world-wide program coordinated by NBS. Program under authority of National Standard Data Act (Public Law 90-396).

Building Science Series—Disseminates technical information developed at the Bureau on building materials, components, systems, and whole structures. The series presents research results, test methods, and performance criteria related to the structural and environmental functions and the durability and safety characteristics of building elements and systems.

Technical Notes—Studies or reports which are complete in themselves but restrictive in their treatment of a subject. Analogous to monographs but not so comprehensive in scope or definitive in treatment of the subject area. Often serve as a vehicle for final reports of work performed at NBS under the sponsorship of other government agencies.

Voluntary Product Standards—Developed under procedures published by the Department of Commerce in Part 10, Title 15, of the Code of Federal Regulations. The purpose of the standards is to establish nationally recognized requirements for products, and to provide all concerned interests with a basis for common understanding of the characteristics of the products. The National Bureau of Standards administers the Voluntary Product Standards program as a supplement to the activities of the private sector standardizing organizations.

Federal Information Processing Standards Publications (FIPS PUBS)—Publications in this series collectively constitute the Federal Information Processing Standards Register. The purpose of the Register is to serve as the official source of information in the Federal Government regarding standards issued by NBS pursuant to the Federal Property and Administrative Services Act of 1949 as amended, Public Law 89-306 (79 Stat. 1127), and as implemented by Executive Order 11717 (38 FR 12315, dated May 11, 1973) and Part 6 of Title 15 CFR (Code of Federal Regulations). FIPS PUBS will include approved Federal information processing standards information of general interest, and a complete index of relevant standards publications.

Consumer Information Series—Practical information, based on NBS research and experience, covering areas of interest to the consumer. Easily understandable language and illustrations provide useful background knowledge for shopping in today's technological marketplace.

NBS Interagency Reports—A special series of interim or final reports on work performed by NBS for outside sponsors (both government and non-government). In general, initial distribution is handled by the sponsor; public distribution is by the National Technical Information Service (Springfield, Va. 22151) in paper copy or microfiche form.

Order NBS publications (except Bibliographic Subscription Services) from: Superintendent of Documents, Government Printing Office, Washington, D.C. 20402.

BIBLIOGRAPHIC SUBSCRIPTION SERVICES

The following current-awareness and literature-survey bibliographies are issued periodically by the Bureau:

Cryogenic Data Center Current Awareness Service (Publications and Reports of Interest in Cryogenics). A literature survey issued weekly. Annual subscription: Domestic, $20.00; foreign, $25.00.

Liquefied Natural Gas. A literature survey issued quarterly. Annual subscription: $20.00.

Superconducting Devices and Materials. A literature survey issued quarterly. Annual subscription: $20.00. Send subscription orders and remittances for the preceding bibliographic services to the U.S. Department of Commerce, National Technical Information Service, Springfield, Va. 22151.

Electromagnetic Metrology Current Awareness Service (Abstracts of Selected Articles on Measurement Techniques and Standards of Electromagnetic Quantities from D-C to Millimeter-Wave Frequencies). Issued monthly. Annual subscription: $100.00 (Special rates for multi-subscriptions). Send subscription order and remittance to the Electromagnetic Metrology Information Center, Electromagnetics Division, National Bureau of Standards, Boulder, Colo. 80302.